Erasmus University Rotterdam
Erasmus School of Economics
Master Thesis Econometrics & Management Science

Manage energy price risks with regime switching GJR-GARCH and regular vine copulas

Cédric Terwel (475378)

Supervisor:	dr. A.M. Camehl
Second assessor:	prof. dr. P.H.B.F. Franses
Date final version:	25th August 2023

Abstract

This study proposes two novel models to capture typical energy commodity price characteristics. Both models combine GJR-GARCH volatilities with regular vine copulas to jointly model the corresponding standardized residuals. The MS-GJR-MS-vine model incorporates Markov switching in both the GJR-GARCH volatilities and vine copula, while the GJR-MS-vine model only makes the standardized residuals regime-switching. I employ these models in forecasting, modelling extreme risks and incorporate them in a multiproduct hedging framework, using daily oil, gas, coal and power prices from January 1, 2015, until June 30, 2023. The MS-GJR-MS-vine model excels in forecasting, while the GJR-MS-vine model effectively captures extreme risks and provides valuable multiproduct hedge strategies that allow an energy consumer to achieve up to 7% extreme risk reduction.

Contents

Chapter 1

Introduction

Since the start of the covid-19 pandemic in early 2020, energy commodity prices in Europe have experienced large fluctuations. The implementation of lockdown measures by several European governments brought the economy to a halt, resulting in a significant reduction in energy demand. For example, oil and gas prices fell by, respectively, 75% and 44% in the period from February to April 2020 (Kuik et al., 2022). At the end of 2020, most energy commodity prices had already reached their pre-pandemic levels. Initially, this rise in energy commodity prices could be attributed to the relaxation of the lockdown measures following the first wave of the covid-19 pandemic, leading to the recovery of economic activity and a subsequent rise in energy demand. In this period, the demand for energy commodities experienced a rebound, as countries tried to recover from the first covid-19 wave. This increase in demand coupled with supply disruptions across various energy sources, contributed to a rally in energy commodities, which in turn amplified the rise in energy commodity prices. This rally in energy commodities was aggravated by the start of the Russo-Ukrainian war on February 24, 2022. Since Russia invaded Ukraine, a lot of political and economic sanctions have been imposed on Russia by, for example, the European Union (EU) and the United States (US) (Ahmed & Hasan, 2022). Russia reacted by setting higher prices and reducing the traded amount of its main export products like wheat, oil and gas (Sokhanvar & Bouri, 2022). Since 27% of crude oil and 41% of natural gas imported by the EU came from Russia, the restrictions caused more price shocks in these products (Eurostat, 2022; Sokhanvar & Bouri, 2022). Due to spillover effects, the restrictions also led to global price shocks in a lot of other commodities (Yagi & Managi, 2023). For example, coal prices experienced an increase of nearly 150% (Nerlinger & Utz, 2022). Such price shocks may have a substantial impact on the economy, as Stern (2000) emphasizes the crucial role of energy as a Gross Domestic Product (GDP) growth factor. He proves the cointegration relationship between energy and GDP and in later studies Stern (2011) finds that, when capital and labor are included in his vector autoregressive model (VAR), energy use also Granger causes GDP. Consequently, not only has the energy market become more risky since the covid-19 pandemic and Russo-Ukrainian war, but as a result of the large fluctuations in energy commodity prices the economies and financial performance of European countries, as well as other continents, can be negatively influenced (Ghorbel & Trabelsi, 2014). Therefore, modelling, forecasting and managing the upside risks that volatile energy commodity prices bring

along, has become a critical issue for governments, regulators and companies in anticipating high energy prices and economically bad times.

When modelling energy commodity prices, one has to take their typical characteristics into account. Energy prices are characterized by a number of features that make them distinct from other types of financial data. For example, energy prices are often highly correlated, exhibit high volatility and are subject to seasonality (Suenaga & Smith, 2011). Basetti et al. (2018) tries to capture these characteristics with a combination of an Autoregressive Generalized Autoregressive Conditional Heteroskedasticity (AR-GARCH) type model and a regular vine (R-vine) copula. GARCH is a commonly used starting point to describe the volatility, as it is able to capture most of the nonlinear dynamics and volatility clustering often present in financial return data (Yang & Brorsen, 1992; Jacobsen & Dannenburg, 2003; Tseng & Li, 2012). An R-vine copula is a tree-like copula that captures the dependence structure between variables. Besides the peculiar advantages copulas already possess, vine copulas allow for a multivariate and very flexible dependence structure. However, in their analysis Basetti et al. (2018) observe that the dependence structure between the different energy prices can differ significantly from year to year due to the nature of the data. As their model does not incorporate regime changes, they limit their analysis to one year at a time.

In this paper, I model energy commodity prices in a time-varying manner. Thereby, I extend Basetti et al. (2018) by building a regime-switching combination of GARCH and R-vine copulas. To that end, I analyze the performance along three dimensions. First, I assess the gain in performance in forecasting energy prices. Thereafter, I investigate the ability of the model in modelling the extreme risks associated to energy prices. And, lastly, I study the improvements in hedging the energy commodities mutually. For assesing the performance of the model in forecasting and hedging energy commodities I employ crude oil, natural gas, coal and electricity from Europe. The energy commodity prices are daily-sampled over the period January 1, 2015, until June 30, 2023.

To capture the typical characteristics energy commodity prices possess, I utilize two models. Firstly, I employ a regime-switching combination of Glosten-Jagannathan-Runkle (GJR-)GARCH (Glosten et al., 1993) and an R-vine copula, denoted as MS-GJR-MS-vine. Secondly, from the MS-GJR-MS-vine model I derive a combination of GJR-GARCH and a regime-switching R-vine copula, denoted as, GJR-MS-vine. Unlike GARCH, the GJR-GARCH model captures the asymmetric leverage volatility effect often found in financial return data producing superior fits in return volatilities (Nugroho et al., 2019). The leverage effect refers to the negative relationship between returns and volatility. According to Charles & Darné (2019), the GJR-GARCH model has similar out-of-sample forecasting accuracy as alternative, asymmetric GARCH models, such as threshold GARCH, exponential GARCH and APARCH. Furthermore, I exploit R-vine copulas

for modelling the dependence structures between the energy prices. R-vine copulas have several attractive features. First of all, R-vine copulas are multivariate copulas, enabling the modelling of multiple energy commodities. Besides, unlike the multivariate Gaussian and Student-t copulas, R-vine copulas can capture the asymmetric dependence structures present in energy markets (Cholette et al., 2009; Lahiani, 2017). And, more importantly, R-vine copulas are not constrained by the requirement that the dependence structures between each pair of variables must have the same copula function, as it is a multivariate copula formed by combining standard bivarite copulas and marginal distribution functions in a cascade manner with each bivariate copula representing the dependence structure of a specific pair of variables. This specific construction scheme assures a very flexible dependence structure providing an optimal basis for correctly modelling the different dependence structures between energy prices. These combinations of GJR-GARCH and an R-vine copula (GJR-vine) capture the high volatility and correlation between the energy prices. I make the combinations regime dependent by means of Markov switching (MS) to include the regime switches found by Basetti et al. (2018) in the model. Hamilton's (1988, 1989) MS models can capture regime shifts in economic time series by allowing the combinations to be influenced by a finite number of discrete states. The resulting models are abbreviated as GJR-MS-vine and MS-GJR-MS-vine.

With the GJR-MS-vine and MS-GJR-MS-vine models, I combine the papers of Basetti et al. (2018) and Lee & Lee (2022). Basetti et al. (2018) who use a GARCH-vine model to describe the volatility in one-year forward energy contracts, while Lee & Lee (2022) use a MS real-time GARCH Clayton-Gumbel copula model (MS-RT-MS-CG) to hedge S&P500 indices with oil futures. Real-time GARCH (RT-GARCH), introduced by Smetanina (2017), is a new kind of GARCH model that incorporates a mixture of past and current information in estimating the volatility. Unfortunately, as current information is not yet available in the previous period, RT-GARCH is infeasible in forecasting. Besides, Lee & Lee (2022) model the dependence structure between the S&P500 indices and the oil futures by means of a combined Clayton-Gumbel copula. This Clayton-Gumbel copula combination has the benefit of modelling both upper and lower tail dependence, but it has the disadvantage that it is only suitable in the bivariate case. Summarizing, I improve the GARCH-vine model of Basetti et al. (2018) by substituting the GARCH volatility model for a GJR-GARCH model and making the model regime-switching as in Lee & Lee (2022). In estimating, I extend the stepwise expectation-maximization (EM) algorithm introduced by Stöber & Czado (2014) with the log-likelihood evaluation technique for vine copulas proposed by Aas et al. (2009) and incorporate the optimization of the GJR-GARCH volatilities within the algorithm.

As a first application of the GJR-MS-vine and MS-GJR-MS-vine models, I make one-day-ahead forecasts of the energy commodity prices and check the gain in performance compared to

their benchmark models. I set a one-regime combination of GJR-GARCH and vine copula (GJR-vine) proposed by Aloui & Aïssa (2016), a Markov-switching GJR-GARCH (MS-GJR) introduced by Cholette et al. (2019) and a regime-switching vine copula (MS-vine) implemented by Zheng (2015) as benchmarks and utilize the forecast bias (FB), mean absolute error (MAE) and the mean squared prediction error (MSPE) as performance indicators. Subsequently, employing the GJR-MS-vine and MS-GJR-MS-vine models, I study how to hedge the price risks in energy prices. Literature in the field of energy commodity hedging has primarly been concentrated on obtaining minimum-variance or mean-variance hedge ratios (Hung et al., 2011; Ahmad et al., 2018; Wang et al., 2019). Because I am solely concerned with the upside risks of the energy commodities and the energy returns show asymmetric and non-normal behaviour, the variance is an improper measure of risk (Harris & Shen, 2006). Instead, I follow Suckharoen & Leatham (2017) who propose a multiproduct futures hedging model that minimizes the value-at-risk (VaR) and expected shortfall (ES). I extend this multiproduct futures hedging model to hedge the energy commodities with each other, instead of using futures, and it takes four energy variables as input. Before employing the multiproduct hedging model, I perform an in-sample analysis on whether the GJR-MS-vine and MS-GJR-MS-vine models correctly model the VaR and ES of the energy commodity pairs. After, I obtain the minimum-VaR and ES hedge ratios using simulated return distributions from the models and employ these out-of-sample.

This research further contributes to the existing literature by the novel GJR-MS-vine and MS-GJR-MS-vine models and the corresponding estimation method: the stepwise EM-algorithm.. The models distinguish themself from previous research that only worked with a regime-switching R-vine copula (Zheng, 2015; Fink et al, 2017) or a regime-switching GJR-GARCH model with or without an uncoupled R-vine copula (Aloui & Aïssa, 2016; Cholette et al., 2019; Mwamba & Mwambi, 2021). Secondly, as an additional contribution to literature I enhance the stepwise EM-algorithm proposed by Stöber & Czado (2014) by incorporating GJR-GARCH volatilities and integrating the log-likelihood evaluation technique developed by Aas et al. (2009).

The novel MS-GJR-MS-vine model shows superior forecasting performance compared to the GJR-MS-vine model and their benchmark models for most energy commodities. However, when modelling the VaR and ES for pairs of energy commodities, the MS-GJR-MS-vine is inaccurate. However, the GJR-MS-vine model and the GJR-vine benchmark model, which perform poorly in forecasting, do effectively capture these risks, making them useful for multiproduct hedging of energy commodity pairs. By employing these two models in combination with minimum-VaR and ES hedging, hedge strategies are developed that lead to up to a 7% reduction in the VaR or ES.

The remainder of this paper is structured as follows. I briefly discuss the literature related to the modelling and forecasting of energy prices in Section 2. Section 3 describes the data for

the empirical research. Section 4 presents the theory behind the GJR-MS-vine and MS-GJR-MS-vine models, their estimation processes and how they are integrated with the multiproduct hedging model. The results are then presented in Section 5. Lastly, Section 6 concludes, discusses limitations and suggests potential areas for further research.

Chapter 2

Literature

A lot of research has been done on modelling and forecasting energy commodity prices and over the years various models have been proposed to capture their volatility dynamics. Since Bollerslev (1986) introduced the GARCH model, this has been the basis of a lot of financial researches in modelling volatility, because it is easily estimated and yields good results, while capturing nonlinear dynamics and volatility clustering. Cheong (2009) takes advantage of these properties when modelling crude oil markets using GARCH, Fractionally Integrated (FI) GARCH, Asymmetric Power (AP) ARCH and FIAPGARCH (Ding et al., 1993; Baillie et al., 1996; Tse, 1998) and he examines their out-of-sample forecasting performance. He finds that the long-persistence volatility in crude oil is best captured by APARCH. On the other hand, Marimoutou et al. (2009) compare the performance of GARCH to extreme value theory (EVT) models in measuring the Value-at-Risk (VaR) in oil markets. VaR is a widely used risk measure that evaluates the risk exposure at a specific probability level and brings it down to only one number (Linsmeier & Pearson, 2000), and EVT explicitly models the tails of the return distribution. EVT and VaR may proof useful in, respectively, modelling price spikes and quantifying the corresponding risks in the oil market. Marimoutou et al. (2009) find that a GARCH model with Student-t distributed residuals measures the VaR equally good. Chan & Gray (2006) combine Exponential GARCH (EGARCH) with EVT in determining the VaR for daily electricity prices and they find that their proposed EGARCH-EVT method provides the most precise VaR forecasts. Since EVT focuses on the tails of the return distribution, it is useful in estimating extreme risk measures, but not in estimating a whole distribution or in forecasting. Hence, Cifter (2013) takes on a different approach and combines MS with GARCH to forecast price volatility in the Nordic electricity market. He distinguishes between

a high and low volatility state and has two main conclusions. First, he observes that electricity prices are strongly regime-dependent and, second, his MS-GARCH model outperforms the normal GARCH and GJR-GARCH in terms of forecasting.

While these univariate GARCH models can effectively model the volatility dynamics of individual energy prices, they do not provide insight into the relationship among energy commodities. Wang & Wu (2012) fill this gap in the literature by exploring the effectiveness of univariate and multivariate GARCH-class models in forecasting West Texas Intermediate (WTI) crude oil, conventional gasoline, heating oil and jet fuel. They find that the multivariate GARCH models are superior in forecasting energy price volatility, as they also capture the comovements in the energy prices.

However, Grégoire et al. (2008) point out that multivariate GARCH models may not accurately capture the nonlinear relationships that exist between energy prices. They propose a more flexible, bivariate approach, which encompasses forecasting crude oil and natural gas prices using a combination of GARCH models and copulas. Copulas are more flexible compared to multivariate GARCH, as they allow for the modelling of any marginal distribution without imposing any restrictions on the joint distribution.

Although there exists a wide range of bivariate copulas, such as the normal, Gumbel and Clayton copulas (Gumbel, 1960; Clayton, 1978), not a lot of higher-dimensional copulas exist. For higher-dimensional copulas one has to resort to elliptical copulas, such as the Gaussian and Student-t copula, which both fail to capture the asymmetric dependence structures present in energy markets (Lahiani, 2017), or to multivariate, non-elliptical construction schemes. Fisher et al. (2009) assess in an empirical analysis the performances of four multivariate non-elliptical copula classes (Koehler-Symanowski by Koehler & Symanowski (1995), Archimedean by Nelsen (2006), multiplicative Liebscher by Liebscher (2006) and pair-copula decomposition) and they compare these to the multivariate Student-t benchmark copula. They find that R-vine copulas (Bedford & Cooke, 2001; Bedford & Cooke, 2002) from the pair-copula decomposition class have the best fit in modelling German bonds, exchange rates and metal commodity futures. This finding is explained by the typical feature that R-vine copulas are not constrained by the requirement that the dependence structures between each pair of variables must have the same copula function, in contrast to most multivariate, non-elliptical copulas. Aloui & Aïssa (2016) apply a regular vine copula in combination with GARCH to investigate the relationship between energy, stock and currency markets and compute the joint VaR. Besides a significant, time-varying and symmetric relationship between these three markets, they find evidence that suggests the application of a vine copula model enhances the accuracy of the VaR estimates compared to conventional approaches. However, not only in the energy market have regular vines, either made regime-dependent through

Markov switching or not, been applied successfully, but also on other kinds of financial data, like exchange rates, volatility indices and equity indices for continents (Cholette et al., 2009; Stöber & Czado, 2014; Fink et al., 2017).

Chapter 3

Data

To examine the influence of R-vine copulas in modelling, forecasting and hedging European energy commodities, I obtain the daily spot prices for oil, gas, coal and power from the Eikon databases provided by the Erasmus University Rotterdam. The sample period ranges from January 1, 2015, until June 30, 2023 (2217 observations). As a proxy for the European oil prices, Brent Crude oil is employed. Brent Crude oil is considered an European oil benchmark as it is gained from the North Sea and distributed not only across Europe, but also across the rest of the world. US dollars (USD) are involved in purchasing Brent Crude oil on the Intercontinental Exchange (ICE). The gas prices are obtained from the Dutch Title Transfer Facility (TTF) market. Here only futures prices are traded, so as a proxy for the spot price I use the one day ahead futures prices in Great Britain Pounds (GBP) for the purchase of 1 megawatt hour (MWh) gas. Furthermore, spot prices on coal are also obtained from the ICE, where coal with destination Rotterdam, Amsterdam and Antwerpen is traded as well. Here prices are in USD per metric tonne. Lastly, for power I utilize the Physical Electricity Index (Phelix) baseload spot prices in euro (EUR) per Megawatt hour obtained from the European Power Exchange (EPX) where power is traded for the Great Britain market area. Baseload power refers to the minimum amount of electric power needed to be supplied to the electrical grid at any given time. The four aforementioned energy commodities are displayed in Figure 3.1 and the corresponding descriptive statistics are listed in Tables A.1 and A.2 and Figure A.1 in Appendix A. Appendix A further emphasizes the typical characteristics of energy commodity prices. Here it is demonstrated that the four energy commodities are very volatile, highly correlated and they are prone to seasonality in the period from January 1, 2015, until June 30, 2023.

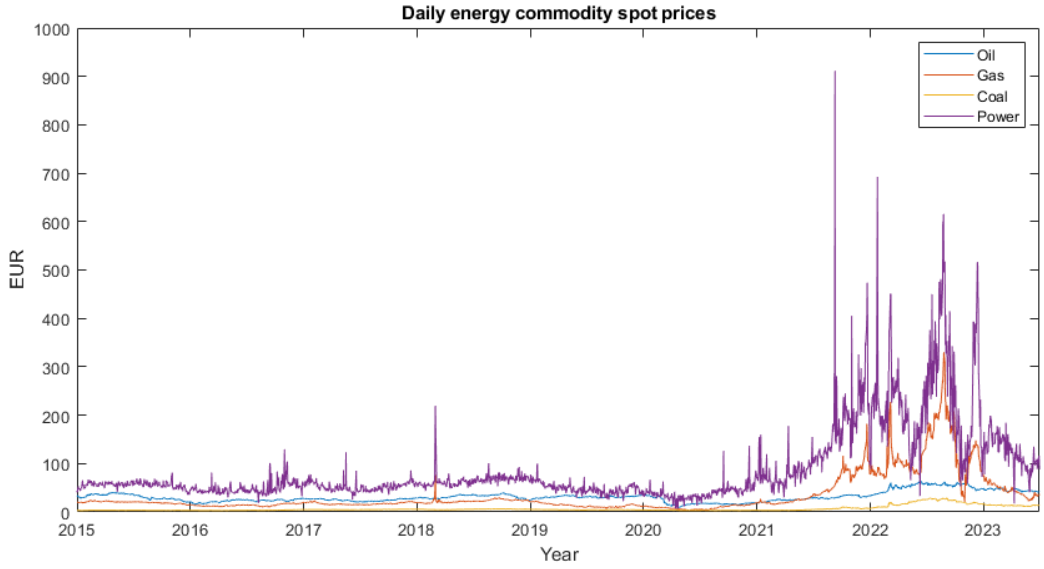

Figure 3.1: Daily energy commodity spot prices of Brent crude oil, gas, coal and baseload power over the period 1 January 2015 until 30 June 2023.

In Figure 3.1 a couple of observations stand out. First of all, around March 1 2018 a high peak in electricity and gas prices is observed. This peak is explained by the freezing cold in West-Europe, falling out of Norwegian production and because only 20% of the gas storages was filled (Kotek et al., 2018). So a shortage of gas occured, while more gas was demanded. This drove gas prices up. The increasing gas prices caused the electricity prices to rise as well (Kotek et al., 2018). Furthermore, Figure 3.1 shows that all energy commodity prices dropped substantially since the start of the pandemic in February 2020. After relaxing the lockdown measures of the first covid-19 wave most energy commodity prices already reached their pre-pandemic levels at the end of 2020. This rise in energy commodity prices carried on in 2021, due to the start of the Russo-Ukrainian war, the import and export restrictions imposed on Russia and other supply disruptions. Moreover, the first half of 2023 is a more stable period, compared to the two years before. However, the price level still remains relatively high when comparing it to the period 2015 until 2021.

To be consistent across the energy commodities and to assign a clear economic interpretation to the purpose of the models and the forthcoming results, I convert the energy commodities to the same currency and unit of measurement. Therefore, gas and coal prices are converted from USD and GBP to EUR using the US/EUR and GBP/EUR exchange rates in the period from January 1, 2015, until June 30, 2023. Additionally, I adjust all energy commodity prices to represent 1 MWh of energy. For instance, I convert Brent Crude oil, traded in barrels, to represent 1.6282 MWh of energy, while I adjust a metric tonne of coal to reflect 8.141 MWh of energy (Dahiya, 2020). After this conversion, I set the energy prices such that they represent 1 MWh of energy. Table 3.1 presents the descriptive statistics of the absolute returns in EUR for holding 1 MWh of

energy, which are calculated as

$$r_{i,t} = P_{i,t} - P_{i,t-1}, \tag{3.1}$$

where $r_{i,t}$ is the absolute return of energy commodity i at time t and $P_{i,t}$ is the spot price of energy commodity i at time t. Table 3.1 shows the descriptive statistics of the returns for the four energy commodities.

Table 3.1: Descriptive statistics of the simple returns in percentages of energy commodity spot prices over the period January 1, 2015, until June 30, 2023.

	Sample size	Mean	St. Dev.	Min.	Max.	Skewness	Kurtosis
Oil	2216	0.004	0.832	-8.094	4.342	-0.753	9.277
Gas	2216	0.007	5.253	-60.250	52.050	-0.377	44.372
Coal	2216	0.005	0.289	-3.671	5.536	2.899	97.197
Power	2216	0.020	35.297	-761.482	624.657	-1.186	164.710

A few things should be noted from Table 3.1. Firstly, the energy returns exhibit small means and relatively high standard deviations. Particularly, the gas and power returns are extremely volatile. These two energy commodities exhibit exceptionally low minima and high maxima, explained by the fact that of the energy prices, especially the gas and power prices skyrocketed since the start of the energy crisis. Consequently, this is a first indication of non-normal data, which is further substantiated by the non-normal skewnesses and kurtoses. Performing a Jarque-Bera test proves that the hypothesis of normality is rejected with a probability of 1 for all variables. Moreover, there are low, yet positive correlations among the energy returns, displayed in Table 3.2, paving the way for the MS-GJR-MS-vine model.

Table 3.2: Correlations between the energy commodity price returns over the period January 1, 2015, until June 30, 2023.

	Oil	Gas	Coal	Power
Oil	1.000	0.129	0.222	0.028
Gas	0.129	1.000	0.391	0.129
Coal	0.222	0.391	1.000	0.061
Power	0.028	0.129	0.061	1.000

Chapter 4

Methodology

The methodology consists of four subsections. First of all, Section 4.1 provides an explanation of the MS-GJR-MS-vine model in its entirety, including its estimation process and the derivation of

the GJR-MS-vine. Next, Section 4.2 describes how to employ the GJR-MS-vine and MS-GJR-MS-vine models in forecasting. Section 4.3 combines the models with a multiproduct hedging model and, lastly, Section 4.4 clarifies the benchmark models against which the performances of the GJR-MS-vine and MS-GJR-MS-vine model are evaluated.

4.1 Markov switching GJR-GARCH R-vine copula model

This section explains the setup and estimation of the novel Markov-switching GJR-GARCH & R-vine copula (MS-GJR-MS-vine) model. The model employs state-dependent GJR-GARCH volatility dynamics to model the univariate margins of the energy spot returns and state-dependent R-vine copula functions are used to capture the dependence structures between the corresponding standardized residuals.

Starting with the univariate margins of the energy spot returns, I follow the energy return forumulation by Laporta et al. (2018). Let $r_{i,t}$ be the energy price return for energy commodity i at time t and be defined as

$$\begin{aligned} r_{i,t} &= \mu_{i,S_t} + \epsilon_{i,t} \\ &= \mu_{i,S_t} + \sigma_{i,S_t,t} z_{i,t} \end{aligned} \tag{4.1}$$

with state-dependent mean μ_{i,S_t} and time-dependent residuals $\epsilon_{i,t}$. The residuals can be decomposed in the volatility $\sigma_{i,S_t,t}$ and standardized residuals $z_{i,t} \sim \text{i.i.d.}(0,1)$, since they are defined as $\epsilon_{i,t} \sim N(0, \sigma^2_{i,St,t})$. The volatilities $\sigma_{i,S_t,t}$ follow a state-dependent GJR-GARCH volatility process (Glosten et al., 1993)

$$\sigma^2_{i,S_t,t} = \alpha_{0,i,S_t} + \sum_{j=1}^{p} (\alpha_{j,i,S_t} + \gamma_{j,i,S_t} \mathbb{1}[r_{i,t-j} < 0]) r^2_{i,t-j} + \sum_{k=1}^{q} \beta_{k,i,S_t} \sigma^2_{i,t-1}. \tag{4.2}$$

By combining Equations 4.1 and 4.2, the marginal pdf of return $r_{i,t}$, conditional on the state S_t and information set $\mathcal{I}_{t-1}$, becomes

$$f(r_{i,t}|S_t, \Psi^i_{GJR,S_t}) = \mu_{i,S_t} + \sigma_{i,S_t,t} f(z_{i,t}), \tag{4.3}$$

where Ψ^i_{GJR} represents the parameter set for return i calculated through GJR-GARCH volatilities Following Lee & Lee (2022) and Fink et al. (2017), I assume the energy prices to be in either a high or a low volatility regime. In other words, I assume the latent state variable S_t to follow a

first-order, two-state Markov chain with transition probability matrix

$$\mathbf{P} = \begin{pmatrix} P[S_t = 1|S_t = 1] & P[S_t = 2|S_t = 1] \\ P[S_t = 1|S_t = 2] & P[S_t = 2|S_t = 2] \end{pmatrix} = \begin{pmatrix} p_{11} & 1 - p_{11} \\ 1 - p_{22} & p_{22} \end{pmatrix}, \tag{4.4}$$

with unconditional state probability, $P[S_t = k|\mathbf{\Psi}_{MS}]$, and conditional state probability, $P[S_t = k|\mathcal{I}_{t-1}, \mathbf{\Psi}]$, for $k \in \{1, 2\}$. Moreover, $\mathbf{\Psi} = \{\mathbf{\Psi}_{GV}, \mathbf{\Psi}_{MS}\}$ represents the complete parameter set of the MS-GJR-MS-vine model, with $\mathbf{\Psi}_{MS}$ specifically denoting the subset of parameters required for the Markov chain. For both the unconditional and conditional state probabilities the sum over the two regimes at time t adds up to 1. With the conditional state probabilities and the law of conditional probability, I define the unconditional marginal pdf of the return $r_{i,t}$ as

$$\begin{aligned} f(r_{i,t}|\mathbf{\Psi}^i) &= \sum_{k=1}^{2} f(r_{i,t}, S_t = k|\mathbf{\Psi}^i) \\ &= \sum_{k=1}^{2} f(r_{i,t}|S_t = k, \Psi^i_{GJR,k}) \times P[S_t = k|\mathbf{\Psi}_{MS}] \\ &= \sum_{k=1}^{2} (\mu_{i,k} + \sigma_{i,k,t} f(z_{i,t})) \times P[S_t = k|\mathbf{\Psi}_{MS}], \end{aligned} \tag{4.5}$$

with $\mathbf{\Psi}^i = \{\Psi^i_{GJR}, \mathbf{\Psi}_{MS}\}$

In addition to the regime-weighted univariate margins of the energy commodity prices, the MS-GJR-MS-vine model further consists of a state-dependent R-vine copula in order to capture the dependence structure between the energy returns through the standardized residuals. This innovative combination distinguishes the MS-GJR-MS-vine model from the existing literature. The standardized residuals $z_{i,t}$ are transformed to uniform variables using the corresponding CDF to make them suitable as input for the R-vine copula: $u_{i,t} = F(z_{i,t})$, $u_{i,t} \in [0, 1]$. Besides, consider a state-dependent R-vine copula $(\mathcal{V}, \mathbf{C}, \mathbf{\Psi}_{vine})_{S_t}$, where $\mathcal{V}$ is the respective tree structure and $\mathbf{C}$ is the set of corresponding bivariate copulas with the parameters stored in the vector $\mathbf{\Psi}_{vine} = \{\Psi^1_{vine}, \ldots, \Psi^n_{vine}\}$. Hence, the 4-dimensional pdf of the standardized residuals of the energy returns can be represented as a state-dependent R-vine copula $c(.|(\mathcal{V}, \mathbf{C}, \mathbf{\Psi}_{vine})_{S_t})$ (Stöber & Czado, 2014)

$$f(z_{1,t}, \ldots, z_{n,t}|\mathbf{\Psi}_{vine,S_t}) = c(u_{1,t}, \ldots, u_{n,t}|(\mathcal{V}, \mathbf{C}, \mathbf{\Psi}_{vine})_{S_t}). \tag{4.6}$$

Combining the unconditional marginal pdf's of the returns $r_{i,t}$, $i \in \{1, ..., n\}$, from Equation 4.5 with the 4-dimensional pdf of the standardized residuals of the energy returns from Equation 4.6 and assuming that the returns are only correlated through the standardized residuals, such that the covariances between the returns are all equal to zero, I propose the n-dimensional pdf of the

returns in the MS-GJR-MS-vine model

$$
\begin{aligned}
f\left(\mathbf{r}_t|\mathbf{\Psi}\right) &= \sum_{k=1}^{2} f(\mathbf{r}_t, S_t = k|\mathbf{\Psi}) \\
&= \sum_{k=1}^{2} f(\mathbf{r}_t|S_t = k, \mathbf{\Psi}_{GV,k}) \times P[S_t = k|\mathbf{\Psi}_{MS}] \\
&= \sum_{k=1}^{2} \Big[\boldsymbol{\mu}_k + \text{Diag}\left(\boldsymbol{\sigma}_{k,t}\right) \times c\Big(\boldsymbol{u}_t|S_t = k, (\mathcal{V}, \mathbf{C}, \mathbf{\Psi}_{vine})_k\Big)\Big] \times P[S_t = k|\mathbf{\Psi}_{MS}],
\end{aligned} \tag{4.7}
$$

with $\mathbf{\Psi} = (\mathbf{\Psi}_{GV}, \mathbf{\Psi}_{MS})$ the complete parameter set, which is composed of two subsets: $\mathbf{\Psi}_{GV} = (\mathbf{\Psi}_{GV,1}, \mathbf{\Psi}_{GV,2})$ represents the parameters from the GJR-GARCH volatilities combined with the vine copula (GJR-vine) for each state $S_t \in \{1, 2\}$, and $\mathbf{\Psi}_{MS}$ represents the parameters specific to the Markov chain. The complete pdf of the MS-GJR-MS-vine model is thus specified in terms of regime-dependent means $\boldsymbol{\mu}_k$, GJR-GARCH volatilities $\boldsymbol{\sigma}_k$, standardized residuals interconnected through a regime-dependent R-vine copula denoted as $c(.|(\mathcal{V}, \mathbf{C}, \mathbf{\Psi}_{vine})_{S_t})$, and unconditional probabilities of being in state k at time t.

4.1.1 Determination of best-fitting R-vine copula

Since multiple vine copulas exists, I make a distinction between two populair R-vine copulas, namely the canonical and the drawable vine copulas (respectively, C- and D-vine). The difference between the C- and D-vine is in the construction of their respective tree structure $\mathcal{V}$. In a C-vine, the pair-copulas are arranged in a specific canonical order, often based on Kendall's tau rank correlation matrix, such that in each tree of the C-vine structure there exists one node that is connected to all other nodes. On the other hand, in each tree of a D-vine, every node has a maximum of two edges. For illustration purposes, the derivations of 4-dimensional, conditional probability density functions for both the C- and the D-vine structures are provided in Appendix B. Additionally, in Appendix C the corresponding 4-dimensional structures are depicted and the distinction between the C- and D-vine becomes even more clear.

I follow the procedure of Sukcharoen & Leatham (2017) in identifying a suitable joint distribution function for the data using the C- and D-vine copula. This process can be summarized in two steps.

1. First, I select an order for the variables in the C- and D-vine copula structures. In the C-vine copula structure, the variable with the highest degree of association (DoA) with all other variables is selected as the first variable. Subsequently, the variable with the highest DoA with the remaining variables is selected, and so on. The DoA for each variable i is measured by summing the absolute values of the pairwise Kendall's tau coefficients: $DoA_\tau^i =$

$\sum_{j=1,i\neq j}^{n} |\tau_{i,j}|$. For the D-vine copula structure, the variables are ordered such that the sum of the absolute values of the pairwise Kendall's tau coefficients is maximized: $DoA_\tau = \sum_{i=1}^{n-1} |\tau_{i,i+1}|$.

2. To determine the bivariate copula for each pair-copula, I employ criteria such as the log-likelihood, Akaike Information Criteration (AIC) and Bayesian Information Criterion (BIC). These criteria assist in selecting the most appropriate bivariate copula based on the goodness-of-fit measures and the complexity of the model.

In determining the vine structures, I make a distinction between the high and low volatility state. Consequently, I expect the vine copulas to be different between the two states $S_t \in \{1, 2\}$ in terms of the structure $\mathcal{V}_{S_t}$, the set of bivariate copulas $\mathbf{C}_{S_t}$ and the corresponding parameters $\mathbf{\Psi}_{vine,S_t}$.

4.1.2 Estimation

In estimating the MS-GJR-MS-vine model, I follow Stöber & Czado (2014) and first derive the full likelihood of a time series of energy return observations $\tilde{\mathbf{r}}_T = (\mathbf{r}_1, \ldots, \mathbf{r}_T)$

$$\begin{aligned} f(\tilde{\mathbf{r}}_T|\mathbf{\Psi}) &= f(\mathbf{r}_1|\mathbf{\Psi}) \cdot \prod_{t=2}^{T} f(\mathbf{r}_t|\tilde{\mathbf{r}}_{t-1}, \mathbf{\Psi}) \\ &= \left[\sum_{k=1}^{2} f(\mathbf{r}_1|S_1 = k, \mathbf{\Psi}_{GV,k}) P[S_1 = k|\mathbf{\Psi}_{MS}]\right] \cdot \prod_{t=2}^{T} \left[\sum_{k=1}^{2} f(\mathbf{r}_t|S_t = k, \mathbf{\Psi}_{GV,k}) \cdot P[S_t = k|\tilde{\mathbf{r}}_{t-1}, \mathbf{\Psi}]\right], \end{aligned} \tag{4.8}$$

and the full likelihood of the joint distribution of energy returns $\tilde{\mathbf{r}}_T$ and states $\tilde{\mathbf{S}}_T = (\mathbf{S}_1, \ldots, \mathbf{S}_T)$

$$f(\tilde{\mathbf{r}}_T, \tilde{\mathbf{S}}_T|\mathbf{\Psi}) = \prod_{t=1}^{T} \left[\sum_{k=1}^{2} (f(\mathbf{r}_t|S_t = k, \mathbf{\Psi}_{GV,k}) \cdot P[S_t = k|\mathbf{\Psi}_{MS}])^{I_{[S_t=k]}}\right]. \tag{4.9}$$

The number of parameters in $\mathbf{\Psi}$ can get increasingly large. The total number of parameters in the complete parameter set $\mathbf{\Psi}$ can be determined with the function

$$Q(n, m) = 10n + n(n-1)m + 4, \tag{4.10}$$

where n is the number of variables and m the number of parameters per bivariate copula inside the vine copula. For example, in case the MS-GJR-MS-vine model consists of four variables and one parameter per bivariate copula the total number of parameters is 56. Because of the size of the parameter set, maximum likelihood estimation (MLE) may pose problems. For example, the likelihood function may have multiple maxima or be very flat in some regions of the parameter space. In addition to this, there is a higher risk at overfitting, identifiability issues or the

possibility of optimization algorithms failing to converge (Boomsma, 1985). Therefore, I employ the expectation-maximization (EM) algorithm as in Cholette et al. (2009) and Stöber & Czado (2014). The EM-algorithm calculates the parameter estimates $\boldsymbol{\Psi}^c, c = 1, 2, \ldots,$ in an iterative manner, such that the parameter estimates converge to the ML estimate for $c \to \infty$, under several regularity conditions. The EM-algorithm iterates through the two-step estimation procedure in Table 4.1.

Table 4.1: Expectation-Maximization algorithm for the MS-GJR-MS-vine model.

Step	**Explanation**
Expectation	Take the expectation of the pseudo log-likelihood function with respect to $S_T\|\tilde{\mathbf{r}}_T$ given $\boldsymbol{\Psi}^c$: $\mathrm{E}_{S_T\|\tilde{\mathbf{r}}_T,\boldsymbol{\Psi}^c}\left[\ln\left(f(\tilde{\mathbf{r}}_T, \tilde{\mathbf{S}}_T\|\boldsymbol{\Psi}^c)\right)\right] = A + B$, where $A = \sum_{t=1}^{T}\Big[\sum_{k=1}^{2} P[S_t = k\|\tilde{\mathbf{r}}_T, \boldsymbol{\Psi}^c]\Big(\ln\left(f(\mathbf{r}_t\|S_t = k, \boldsymbol{\Psi}^c_{GV,k})\right)\Big)\Big]$ $B = \sum_{t=1}^{T}\Big[P[S_t = 1\|\tilde{\mathbf{r}}_T, \boldsymbol{\Psi}^c]\ln\Big(P[S_t = 1\|\boldsymbol{\Psi}^c_{MS}]\Big)$ $+\Big(1 - P[S_t = 1\|\tilde{\mathbf{r}}_T, \boldsymbol{\Psi}^c]\Big)\ln\Big(1 - P[S_t = 1\|\boldsymbol{\Psi}^c_{MS}]\Big)\Big]$. Afterwards, obtain the conditional probabilities of the unobserved states $\tilde{\mathbf{S}}_T = (S_1, \ldots, S_T)$ given the current parameter set $\boldsymbol{\Psi}^c$, i.e. $P[S_t = k\|\tilde{\mathbf{r}}_T, \boldsymbol{\Psi}^c]$, by employing the Hamilton filter (Table E.1, Appendix E).
Maximization	Maximize the expected pseudo log-likelihood function with respect to $\boldsymbol{\Psi}^{c+1}$, where the probability of being in an unobserved state S_t is replaced by the conditional probability from the expectation step, $P[S_t = k\|\tilde{\mathbf{r}}_T, \boldsymbol{\Psi}^c]$, $\max_{\boldsymbol{\Psi}^{c+1}}\Big\{\mathrm{E}_{S_T\|\tilde{\mathbf{r}}_T,\boldsymbol{\Psi}^c}\left[\ln\left(f(\tilde{\mathbf{r}}_T, \tilde{\mathbf{S}}_T\|\boldsymbol{\Psi}^{c+1})\right)\right]\Big\} = C + D$, where $C = \max_{\boldsymbol{\Psi}^{c+1}_{GV}}\Big\{\sum_{t=1}^{T}\Big[\sum_{k=1}^{2} P[S_t = 1\|\tilde{\mathbf{r}}_T, \boldsymbol{\Psi}^c]\Big(\ln\left(f(\mathbf{r}_t\|S_t = k, \boldsymbol{\Psi}^{c+1}_{GV,k})\right)\Big)\Big]\Big\}$ $D = \max_{\boldsymbol{\Psi}^{c+1}_{MS}}\Big\{\sum_{t=1}^{T}\Big[P[S_t = 1\|\tilde{\mathbf{r}}_T, \boldsymbol{\Psi}^c]\ln\Big(P[S_t = 1\|\boldsymbol{\Psi}^{c+1}_{MS}]\Big)$ $+\Big(1 - P[S_t = 1\|\tilde{\mathbf{r}}_T, \boldsymbol{\Psi}^c]\Big)\ln\Big(1 - P[S_t = 1\|\boldsymbol{\Psi}^c_{MS}]\Big)\Big]\Big\}$

To give a better understanding of the EM-algorithm specifically applied to the MS-GJR-MS-vine model, I elaborate on the two steps for an arbitrary iteration c. The first step in the EM-algorithm is the expectation step. Here the expectation of the pseudo log-likelihood is computed for the joint pdf of the energy returns $\tilde{\mathbf{r}}_t$ and states $\tilde{\mathbf{S}}_t$. This expectation is taken with respect to $\mathbf{S}_T|\tilde{\mathbf{r}}_T$ and given the parameter set in the current iteration $\boldsymbol{\Psi}^c$. This expectation can be divided into the expectation of the regime-switching vine copula A and the expectation of the unconditional state probabilities B. See Appendix D for the full derivation of the expected pseudo log-likelihood of the joint energy return and latent state function. After taking the expectation of the pseudo log-likelihood, I obtain the conditional probabilities of the latent states given the current parameter set $P[S_t = k|\tilde{\mathbf{r}}_T, \boldsymbol{\Psi}^c]$ by running through the Hamilton filter outlined in Table E.1, Appendix E.

The second step in the EM-algorithm entails the maximization step, wherein the expected pseudo log-likelihood of the joint energy return and state function parameter set $\mathbf{\Psi}^{c+1}$ is maximized with respect to the parameter set $\mathbf{\Psi}^{c}$. Similarly, this optimization process can be divided into the maximization of the regime-switching vine copula C and the maximization of the unconditional state probabilities D. The latter can be derived analytically (see Appendix F.1).

In Hamilton's original model all maximization steps were analytically solvable. However, in the MS-GJR-MS-vine model, it is not possible to derive the vine copula parameters analytically when maximizing C. This is because vine copulas are not only highly nonlinear, but they consist of multiple connected bivariate copulas which makes analytical solutions unachievable. Consequently, while the transition and unconditional state probabilities can be directly obtained, numerical optimization methods are required to maximize C. Since maximizing C entails maximizing a GJR-vine for both states $S_t \in \{1, 2\}$, a total of $Q(n, m)$ parameters (see Equation 4.10) need to be optimized. Even with the aid of numerical optimization methods, this task remains computationally very challenging. To circumvent this problem, I integrate the stepwise EM-algorithm from Stöber & Czado (2014) with the log-likelihood evaluation technique introduced by Aas et al. (2009) and include the optimization of the GJR-GARCH volatilities within the algorithm. As a result, C is maximized in a stepwise manner. This stepwise maximization is presented in Algorithms 1 and 2. Algorithm 1 outlines the procedure for a regime-switching combination of GJR-GARCH volatilities along with a C-vine to connect the standardized residuals. On the other hand, Algorithm 2 shows the steps for a regime-switching combination of GJR-GARCH volatilities with a D-vine to connect the standardized residuals. See Appendix F.2 for the corresponding log-likelihood functions.

In both Algorithms 1 and 2, I assume a normal distribution, $\phi(\cdot)$, for the GJR-GARCH volatility model. The standardized residuals $\mathbf{z}_i^k$ are transformed into uniform observations $\mathbf{u}_0^k$ through their corresponding empirical distribution functions (EDF) to accomodate the bivariate copula functions. Furthermore, to calculate new observations for the next layer j in the vine structure, the so-called h-function is applied. The h-function is defined as the conditional distribution function of a bivariate copula

$$h(x, v|\Theta) = \frac{\partial C_{x,v}(x, v|\Theta)}{\delta v}. \tag{4.11}$$

Moreover, the parameter set for the GJR-vine at iteration $c+1$, $\mathbf{\Psi}_{GV}^{c+1}$, is decomposed in Appendix F.3.

Stöber & Czado (2014) point out that the convergence properties of the EM-algorithm are lost when approximating the maximization step in the EM-algorithm by stepwise maximization. Limit theorems, such as the Generalized Expectation Maximization theorem introduced by Wu

Algorithm 1 Stepwise maximization of a regime-switching GJR & C-vine

Require: Conditional state probabilities $w_{1,t}^c = P[S_t = 1|\tilde{\mathbf{r}}_T, \mathbf{\Psi}^c]$ and $w_2^c = P[S_t = 2|\tilde{\mathbf{r}}_T, \mathbf{\Psi}^c]$

log-likelihood = 0

for $i \leftarrow 1, \ldots, n$ **do**

Maximize the log-likelihood of the GJR-GARCH model

$$\text{LL} = \max_{\mathbf{\Psi}_{GJR,i}^{c+1}} \left\{ \sum_{t=1}^{T} \Big[w_{1,t}^c \ln\Big(\phi(r_{i,t}|\mu_{i,1}^{c+1}, (\sigma_{i,1,t}^{c+1})^2)\Big) + w_{2,t}^c \ln\Big(\phi(r_{i,t}|\mu_{i,2}^{c+1}, (\sigma_{i,2,t}^{c+1})^2)\Big) \Big] \right\}$$

and obtain the corresponding standardized residuals per state k: $z_{i,t}^k = \frac{r_{i,t}-\mu_{i,k}}{\sigma_{i,k,t}}$, $\forall t$.

log-likelihood = log-likelihood + LL

$\mathbf{u}_{0,i}^k = F(\mathbf{z}_i^k)$, $\forall k$, where $\mathbf{z}_i^k = \Big(z_{i,1}^k, \ldots, z_{i,T}^k\Big)$.

end for

for $j \leftarrow 1, \ldots, n-1$ **do**

for $i \leftarrow 1, \ldots, n-j$ **do**

$$\text{LL} = \max_{\mathbf{\Psi}_{vine,\{j,i\}}^{c+1}} \left\{ \sum_{t=1}^{T} \Big[w_{1,t}^c \ln\Big(c_{j,i}^1(\mathbf{u}_{j-1,1}^1, \mathbf{u}_{j-1,i+1}^1|\Theta_{j,i}^{1,c+1})\Big) + w_{2,t}^c \ln\Big(c_{j,i}^2(\mathbf{u}_{j-1,1}^2, \mathbf{u}_{j-1,i+1}^2|\Theta_{j,i}^{2,c+1})\Big) \Big] \right\}$$

log-likelihood = log-likelihood + LL

end for

if $j == n-1$ **then**

Stop

end if

for $i \leftarrow 1, \ldots, n-j$ **do**

$\mathbf{u}_{j,i}^k = h\left(\mathbf{u}_{j-1,i+1}^k, \mathbf{u}_{j-1,1}^k|\Theta_{j,i}^{k,c+1}\right)$, $\forall k$

end for

end for

(1983), rely on proper maximization at each step of the EM algorithm, which is nearly impossible to guarantee in the case of the MS-GJR-MS-vine model due to its high-dimensionality. Therefore, employing numerical techniques is necessary, making all numerically obtained maximizations approximations. Especially, the stepwise maximization step is a good approximation as it ensures asymptotic consistency. Furthermore, the stepwise maximization procedure helps mitigate the computational burden associated with estimation in existing models for time-varying dependence structures in higher dimensions, as it focuses solely on maximizing the likelihoods of bivariate copulas within a tree-wise procedure. As a result, computation time is reduced, and the curse of dimensionality alleviated.

4.1.3 GJR-MS-vine model

Introducing a second model, I propose a derivative of the MS-GJR-MS-vine model, referred to as the GJR-MS-vine model. While the MS-GJR-MS-vine is a regime-switching combination of GJR-GARCH volatilities and R-vine copula functions, the GJR-MS-vine combines GJR-GARCH volatilities to model the univariate margins of the energy spot returns with Markov-switching

Algorithm 2 Stepwise maximization of a regime-switching GJR & D-vine

Require: Conditional state probabilities $w_{1,t}^c = P[S_t = 1|\tilde{\mathbf{r}}_T, \mathbf{\Psi}^c]$ and $w_2^c = P[S_t = 2|\tilde{\mathbf{r}}_T, \mathbf{\Psi}^c]$

log-likelihood = 0

for $i \leftarrow 1, \ldots, n$ **do**

Maximize the log-likelihood of the GJR-GARCH model

$$\text{LL} = \max_{\mathbf{\Psi}_{GJR,i}^{c+1}} \left\{ \sum_{t=1}^{T} \Big[w_{1,t}^c \ln\Big(\phi(r_{i,t}|\mu_{i,1}^{c+1}, (\sigma_{i,1,t}^{c+1})^2)\Big) + w_{2,t}^c \ln\Big(\phi(r_{i,t}|\mu_{i,2}^{c+1}, (\sigma_{i,2,t}^{c+1})^2)\Big) \Big] \right\}$$

and obtain the corresponding standardized residuals per state k: $z_{i,t}^k = \frac{r_{i,t}-\mu_{i,k}}{\sigma_{i,k,t}}$, $\forall t$.

log-likelihood = log-likelihood + LL

$\mathbf{u}_{0,i}^k = F(\mathbf{z}_i^k)$, $\forall k$, where $\mathbf{z}_i^k = \Big(z_{i,1}^k, \ldots, z_{i,T}^k\Big)$.

end for

for $i \leftarrow 1, \ldots, n-1$ **do**

$$\text{LL} = \max_{\mathbf{\Psi}_{vine,\{1,i\}}^{c+1}} \left\{ \sum_{t=1}^{T} \Big[w_{1,t}^c \ln\Big(c_{1,i}^1(\mathbf{u}_{0,i}^1, \mathbf{u}_{0,i+1}^1|\Theta_{1,i}^{1,c+1})\Big) + w_{2,t}^c \ln\Big(c_{1,i}^2(\mathbf{u}_{0,i}^2, \mathbf{u}_{0,i+1}^2|\Theta_{1,i}^{2,c+1})\Big) \Big] \right\}$$

log-likelihood = log-likelihood + LL

end for

$\mathbf{u}_{1,1}^k = h\Big(\mathbf{u}_{0,1}^k, \mathbf{u}_{0,2}^k|\Theta_{1,1}^{k,c+1}\Big)$, $\forall k$

for $l \leftarrow 1, \ldots, n-3$ **do**

$\mathbf{u}_{1,2l}^k = h\Big(\mathbf{u}_{0,l+2}^k, \mathbf{u}_{0,l+1}^k|\Theta_{1,l+1}^{k,c+1}\Big)$, $\forall k$

$\mathbf{u}_{1,2l+1}^k = h\Big(\mathbf{u}_{0,l+1}^k, \mathbf{u}_{0,l+2}^k|\Theta_{1,l+1}^{k,c+1}\Big)$, $\forall k$

end for

$\mathbf{u}_{1,2n-4}^k = h\Big(\mathbf{u}_{0,n}^k, \mathbf{u}_{0,n-1}^k|\Theta_{1,n-1}^{k,c+1}\Big)$, $\forall k$

for $j \leftarrow 2, \ldots, n-1$ **do**

for $i \leftarrow 1, \ldots, n-j$ **do**

$$\text{LL} = \max_{\mathbf{\Psi}_{vine,\{j,i\}}^{c+1}} \left\{ \sum_{t=1}^{T} \Big[w_{1,t}^c \ln\Big(c_{j,i}^1(\mathbf{u}_{j-1,2i-1}^1, \mathbf{u}_{j-1,2i}^1|\Theta_{j,i}^{1,c+1})\Big) + w_{2,t}^c \ln\Big(c_{j,i}^2(\mathbf{u}_{j-1,2i-1}^2, \mathbf{u}_{j-1,2i}^2|\Theta_{j,i}^{2,c+1})\Big) \Big] \right\}$$

log-likelihood = log-likelihood + LL

end for

if $j == n-1$ **then**

Stop

end if

$\mathbf{u}_{j,1}^k = h\Big(\mathbf{u}_{j-1,1}^k, \mathbf{u}_{j-1,2}^k|\Theta_{j,1}^{k,c+1}\Big)$, $\forall k$

end for

standardized residuals, interconnected through a vine copula. The key distinction between the two models is the fact that the GJR-GARCH volatilities are not regime-switching. The corresponding pdf of the energy returns is as follows.

$$f\left(\mathbf{r}_t|\mathbf{\Psi}\right) = \boldsymbol{\mu} + \text{Diag}\left(\boldsymbol{\sigma}_t\right) \times \left[\sum_{k=1}^{2} P[S_t = k|\mathbf{\Psi}_{MS}] \times c\Big(\boldsymbol{u}_t|S_t = k, (\mathcal{V}, \mathbf{C}, \mathbf{\Psi}_{vine})_k\Big)\right] \tag{4.12}$$

The estimation procedure of the GJR-MS-vine model is closely related to the estimation of the MS-GJR-MS-vine model. Both are estimated by means of the stepwise EM-algorithm. While the expectation step remains consistent across both models, the maximization step differs. Appendix

G presents the modified Algorithms 3 and 4 for stepwise maximizing the GJR-MS-vine model.

4.2 Forecasting

The first application of the GJR-MS-vine and MS-GJR-MS-vine models is in forecasting. Since MS models rely on the assumption that future behaviour of the return series is influenced by its current state, forecasting multiple steps ahead can be very difficult, especially for highly nonlinear MS models, as not only the return series should be predicted, but the sequence of future regime changes as well. Therefore, I focus on the calculation of one-day-ahead forecasts of the energy returns, $E[\mathbf{r}_{T+1}|\tilde{\mathbf{r}}_T, \hat{\mathbf{\Psi}}]$. To assess the forecasting ability of the models, I employ the models in forecasting two distinct periods. The first period exhibits very high volatile energy prices and it ranges from Janary 3, 2022, until June 30, 2022, comprising 129 observations. By contrast, the second period is a relatively stable period and it ranges from January 1, 2023, until June 30, 2023, with a length of 130 days. The forecast results are obtained using all available, previous observations, meaning a rolling window with a length of 7 years for the volatile period and 8 years for the stable period (respectively, 1827 and 2086 observations). So for the second, stable period the observations from January 1, 2015, until December 30, 2022, are employed to train the GJR-MS-vine and MS-GJR-MS-vine models to obtain a reliable prediction of the energy returns on January 1, 2023. Afterwards the estimation window is rolled over 1 observation to forecast the energy returns on January 2, 2023. For each step the best structures for the regime-switching vine copulas in the GJR-MS-vine and MS-GJR-MS-vine models are determined, as explained in Section 4.1.1. Subsequently, the model is estimated via the stepwise EM-algorithm (Section 4.1.2) and all the associated parameters are obtained. Thereafter, I generate $M = 1,000,000$ samples, $\{u_1^k, \ldots, u_n^k\}$, from both regimes in the GJR-MS-vine and MS-GJR-MS-vine models. Applying the inverse EDF, these samples are transformed back into standardized residuals samples for each energy return i

$$z_{i,m}^k = F_i^{-1}(u_{i,m}^k),\ k \in \{1,2\},\ m \in \{1,\ldots,M\}. \tag{4.13}$$

Besides, the estimated GJR-GARCH model is employed to make regime-dependent one-day-ahead volatility forecasts

$$\hat{\sigma}^2_{i,S_{T+1},T+1} = \hat{\alpha}_{0,i,S_{T+1}} + \sum_{j=1}^{p}(\hat{\alpha}_{j,i,S_{T+1}} + \hat{\gamma}_{j,i,S_{T+1}}\mathbb{1}[r_{i,T} < 0])r_{i,T}^2 + \sum_{k=1}^{q}\hat{\beta}_{k,i,S_{T+1}}\sigma_{i,T}^2. \tag{4.14}$$

Subsequently, I acquire the regime-weighted energy returns by combining the sampled standardized residuals $\boldsymbol{z}_m^k = \left(z_{1,m}^k, \ldots, z_{n,m}^k\right)$, the one-day-ahead GJR-GARCH volatility forecasts $\hat{\boldsymbol{\sigma}}^2_{S_{T+1},T+1} = \left(\hat{\sigma}^2_{1,S_{T+1},T+1}, \ldots, \hat{\sigma}^2_{n,S_{T+1},T+1}\right)$ and the conditional state probabilities obtained in the prediction

step of the Hamilton filter in Table E.1, Appendix E. Summing up the regime-weighted energy returns over the two states gives a one-day-ahead energy return forecast

$$E[\mathbf{r}_{T+1}|\tilde{\mathbf{r}}_T, \hat{\mathbf{\Psi}}] = \sum_{k=1}^{2} \left[P[S_{T+1} = k|\tilde{\mathbf{r}}_T, \hat{\mathbf{\Psi}}] \cdot \frac{1}{M} \sum_{m=1}^{M} \left(\hat{\boldsymbol{\mu}}_k + \hat{\boldsymbol{\sigma}}^2_{k,T+1} \boldsymbol{z}^k_m \right) \right]. \tag{4.15}$$

After obtaining the one-day-ahead forecasts, I evaluate the forecasting performance of the models for energy price i over the forecast period [T, T + f]. The forecasting performance is measured through a number of performance measures.

1. The forecast bias (FB) measures the systematic overestimation or underestimation of the forecasted energy returns compared to the actual energy returns. A positive bias indicates that the forecasts are consistently higher than the actual values, while a negative bias indicates consistently lower forecasts.

$$FB_i = \frac{1}{f} \sum_{l=T}^{T+f} \left(P_{i,l+1} - \left(P_{i,l} + E[\mathbf{r}_{i,l+1}|\tilde{\mathbf{r}}_l, \hat{\mathbf{\Psi}}] \right) \right) \tag{4.16}$$

2. The mean absolute error (MAE) calculates the average absolute difference between the forecasted values and the actual values. It provides a measure of the average magnitude of forecast errors, regardless of their direction.

$$MAE_i = \frac{1}{f} \sum_{l=T}^{T+f} \left| P_{i,l+1} - \left(P_{i,l} + E[\mathbf{r}_{i,l+1}|\tilde{\mathbf{r}}_l, \hat{\mathbf{\Psi}}] \right) \right| \tag{4.17}$$

3. The mean squared prediction error (MSPE) calculates the average squared difference between the forecasted energy returns and the actual energy returns. It gives more weight to the large errors compared to the MAE.

$$MSPE_i = \frac{1}{f} \sum_{l=T}^{T+f} \left(P_{i,l+1} - \left(P_{i,l} + E[\mathbf{r}_{i,l+1}|\tilde{\mathbf{r}}_l, \hat{\mathbf{\Psi}}] \right) \right)^2 \tag{4.18}$$

4. The paired t-test is employed to compare the means of two related samples. The test assesses whether the difference between the forecasts of the MS-GJR-MS-vine model X and forecasts generated by any of the benchmark models Y is statistically significant. The null hypothesis of zero mean difference between the forecasts is rejected when the following test statistic becomes too large.

$$t = \frac{\overline{D}}{SE_{\overline{D}}}, \tag{4.19}$$

with sample mean $\overline{D} = \frac{\sum(X-Y)}{n}$ and sample standard error $SE_{\overline{D}}$.

4.3 Multiproduct hedging

In this section I explain the application of the multiproduct futures hedging model of Sukcharoen & Leatham (2017) to the GJR-MS-vine and MS-GJR-MS-vine models and how to modify it to a multiproduct hedging model.

Again, I simulate 10,000 samples of the standard uniform energy price variables, $\{u_1, \ldots, u_n\}$, from both regimes in the model. By applying the inverse EDF to these samples and combining them with simulated volatilities, they are transformed into samples from the joint distribution of energy prices. Subsequently, the sampled energy price volatilities from both regimes are aggregated into regime-weighted energy returns. Next, I utilize the simulated energy spot and futures returns to calculate the energy consumer's hedged profits and losses (P&Ls). Before defining the hedge P&Ls, I make a few assumptions. First, I assume that energy consumers have taken energy futures positions in the previous period $t-1$ and they liquidate all futures positions in the current period t together with buying the energy commodities. Additionally, for simplicity, I assume that any other costs involved are deterministic and thus do not influence hedging decisions. Lastly, the prices at time $t-1$ are known at time t, while the prices at time t are stochastic variables. Since I have not yet specified which energy commodities to hedge or use as hedging instruments, I continue to use numbers for the energy commodities $i \in \{1, 2, 3, 4\}$. According to Sukcharoen & Leatham (2017) with these assumptions and notations, the hedge P&Ls of an energy consumer, who consumes one euro of two energy commodities (either oil, gas, coal and/or electricity) and hedges them with the corresponding energy commodity futures is

$$\pi_t(b_1, b_2) = -r_{1,t} - r_{2,t} + b_1 F_{1,t} + b_2 F_{2,t}, \tag{4.20}$$

where $r_{i,t}$ and $F_{i,t}$ denote, respectively, the spot and futures returns of energy commodity i. Furthermore, b_i is the hedge ratio for energy commodity future i. Extending the multiproduct futures hedging model to a multiproduct hedging model can be easily done by replacing the energy futures for the spot prices of other energy commodities, such that the hedge is done through any of the other energy commodities. And, instead of assuming that the energy consumers consume one euro of two energy commodities, I assume the energy consumers to consume one MWh of two energy commodities to better compare the different energy commodities and what a energy consumer really consumes in terms of energy. The hedge equation than follows

$$\pi_t(b_1, b_2) = -r_{1,t} - r_{2,t} + b_1 r_{3,t} + b_2 r_{4,t}. \tag{4.21}$$

Different hedge equation combinations are possible, as I did not yet specify Equations 4.20 and

4.21. When taking the positions of the energy commodities in Equation 4.21 into consideration, a total of $4! = 24$ different hedge equations can be derived. However, the positions of the returns do not matter, as it is only of interest whether the energy commodities are hedged or are used to hedge. Therefore, to avoid 'duplicate' hedge equation combinations with the same economic interpretation of the hedge ratios, except they are reversed over b_1 and b_2, I only consider the 'distinct' P&L's, leaving me with 6 different hedge combinations.

1. $\pi_t(b_1, b_2) = -r^O_{1,t} - r^G_{2,t} + b_1 r^C_{3,t} + b_2 r^P_{4,t}$
2. $\pi_t(b_1, b_2) = -r^P_{1,t} - r^O_{2,t} + b_1 r^C_{3,t} + b_2 r^G_{4,t}$
3. $\pi_t(b_1, b_2) = -r^P_{1,t} - r^G_{2,t} + b_1 r^C_{3,t} + b_2 r^O_{4,t}$
4. $\pi_t(b_1, b_2) = -r^P_{1,t} - r^C_{2,t} + b_1 r^O_{3,t} + b_2 r^G_{4,t}$
5. $\pi_t(b_1, b_2) = -r^O_{1,t} - r^C_{2,t} + b_1 r^P_{3,t} + b_2 r^G_{4,t}$
6. $\pi_t(b_1, b_2) = -r^G_{1,t} - r^C_{2,t} + b_1 r^O_{3,t} + b_2 r^P_{4,t}$

The energy consumer's objective is to minimize the upside risk of the hedged P&Ls by selecting the optimal hedge ratios (b^*_1, b^*_2). The upside risk is quantified through the popular VaR and ES. The definitions of VaR and ES can be found in Appendix H. These measures traditionally focus on losses, or in other words, the downside risk. However, I am interested in measuring the upside risk of energy commodities. To align with the definitions of VaR and ES and still capture the upside risk, the energy prices are negated by multiplying them with -1. The Nelder-Mead direct search method (Nelder & Mead, 1965) is utilized to determine the optimal hedge ratios by numerically solving the following minimization problems for the VaR of $\pi_t(b_1, b_2)$

$$(b^*_{1,VaR}, b^*_{2,VaR}) = \arg\min_{b_1,b_2}\{VaR_x(\pi_t(b_1, b_2))\}, \tag{4.22}$$

and the ES of $\pi_t(b_1, b_2)$,

$$(b^*_{1,ES}, b^*_{2,ES}) = \arg\min_{b_1,b_2}\{ES_x(\pi_t(b_1, b_2))\}. \tag{4.23}$$

To determine whether the minimum-VaR or ES hedge has been useful and significant, I calculate the hedge effectiveness as a last step. It is measured as the percentage reduction in the upside risk of the portfolio of hedged P&Ls compared to a portfolio of unhedged P&Ls. The hedge effectiveness for the VaR of the hedged P&Ls is calculated as

$$\text{HE}_{VaR} = \left(1 - \frac{VaR_x(\pi_t(b^*_{1,VaR}, b^*_{2,VaR})}{VaR_x(\pi_t(0, 0)}\right) \times 100\%, \tag{4.24}$$

and for the ES of the hedged P&Ls is

$$\text{HE}_{ES} = \left(1 - \frac{ES_x(\pi_t(b^*_{1,ES}, b^*_{2,ES})}{ES_x(\pi_t(0,0)}\right) \times 100\%. \tag{4.25}$$

I make a distinction between an in-sample and out-of-sample analysis in assessing the hedging performance of the GJR-MS-vine and MS-GJR-MS-vine models. In the in-sample analysis, I assess the ability of the models to correctly model the VaR and ES in two steps. First, I generate 1,000,000 simulated energy commodity prices from the models, which are estimated on the full dataset. Second, I set in hedge combinations 1 to 6 both b_1 and b_2 equal to zero and calculate the VaR and ES of the energy consumer's unhedged P&Ls. The unhedged VaR and ES are compared to the actual VaR and ES of the corresponding energy commodity pairs. After completing the in-sample analysis, I proceed to evaluate the two hedging methods on their out-of-sample HE. To achieve this, I employ a rolling window approach as follows. First, I estimate the models on the first 2086 daily observations, covering a period of 8 years, and generate simulated energy commodity prices from the estimated models. Next, I determine the minimum-VaR and ES optimal hedge ratios (HR) on the simulations. Subsequently, these optimal HR are utilized to construct the hedged P&Ls for the following 20 days, corresponding to a period of 1 month. Lastly, I calculate the out-of-sample HE for the models. By repeating these four steps in a rolling window, I obtain a set of 110 HE observations. From this set, I compute the mean and median out-of-sample HE.

4.4 Benchmark models

In this section I elaborate on the probability density functions of the benchmark models against which the proposed GJR-MS-vine and MS-GJR-MS-vine models from Equations 4.12 and 4.7 are compared. These benchmark models serve as a baseline for evaluating the performance of the GJR-MS-vine and MS-GJR-MS-vine models in terms of forecasting and hedging. By comparing the results with the benchmark models, insights into the potential applicability and performance in practical scenarios are provided. The following models serve as benchmark models:

1. Starting with the GJR-vine model (Aloui & Aïssa, 2016), it considers a single regime with GJR-GARCH volatilities and connects the standardized residuals through a vine copula.

$$f\left(\mathbf{r}_t|\mathbf{\Psi}_{GV}\right) = \boldsymbol{\mu} + \text{Diag}\left(\boldsymbol{\sigma}_t\right) \times c\Big(\boldsymbol{u}_t|\left(\mathcal{V}, \mathbf{C}, \mathbf{\Psi}_{vine}\right)\Big) \tag{4.26}$$

2. The MS-vine model, proposed by Cholette et al. (2019), is a four-dimensional regime-

switching vine copula directly modelling the energy commodity returns.

$$f\left(\mathbf{r}_t|\mathbf{\Psi}_{vine},\mathbf{\Psi}_{MS}\right)=\sum_{k=1}^{2}P[S_t=k|\mathbf{\Psi}_{MS}]\times c\Big(\boldsymbol{u}_t|S_t=k,(\mathcal{V},\mathbf{C},\mathbf{\Psi}_{vine})_k\Big) \tag{4.27}$$

3. The MS-GJR model (Zheng, 2015) is a one-dimensional regime-switching GJR-GARCH volatility model. Consequently, the MS-GJR model should be applied separately to each of the n energy commodity returns.

$$f\left(\mathbf{r}_{i,t}|\Psi^i_{GJR},\Psi^i_{MS}\right)=\sum_{k=1}^{2}P[S_t=k|\mathbf{\Psi}_{MS}]\times\Big[\mu_{i,k}+\text{Diag}\left(\sigma_{i,k,t}\right)\times f(z_{i,t})\Big] \tag{4.28}$$

Chapter 5

Results

In this section I elaborate on the results obtained by implementing the methodology from Section 4 into Python 3.9. I start by examining the optimal settings for the MS-GJR-MS-vine model in terms of computation time and forecast reliability in Section 5.1. Subsequently, I evaluate the forecast performances of the GJR-MS-vine and MS-GJR-MS-vine models by comparing them with the benchmark models in Section 5.2. Next, I perform an in-sample analysis of the models in Section 5.3. Thereafter, the results of employing the models in out-of-sample hedging are presented in Section 5.4, where I also draw conclusions whether the GJR-MS-vine and/or MS-GJR-MS-vine model outperform the benchmark models and give recommendations what energy commodities are useful in mutual hedging.

5.1 Check for best settings in model

As described in Section 4.2, I employ the GJR-MS-vine and MS-GJR-MS-vine models in a rolling window to generate forecasts. In each iteration of the rolling window, the stepwise-EM algorithm ideally converges to its optimal parameters. However, parameter convergence is not guaranteed (see Section 4.1), so I aim for log-likelihood convergence. Since convergence may take a while,

its best practice to implement stopping conditions. I implement two stopping conditions for the stepwise-EM algorithm. The algorithm stops either when the change in the log-likelihood between consecutive iterations falls below a prespecified threshold of 0.01 or when the maximum number of iterations (MNoI) has been reached. The MNoI is a choice between computation time and convergence of the stepwise EM-algorithm. To determine the optimal MNoI, I investigate the forecasting performance of the MS-GJR-MS-vine model over the stable period January 1, 2023, until June 30, 2023, (130 forecasts) in terms of MSPE for various MNoIs, and to be consistent I employ the optimal MNoI in the other models as well. The choice for determining the optimal MNoI on the MS-GJR-MS-vine model is motivated by the fact that this model requires the longest computation time, which should therefore be truncated. Table 5.1 presents these results. As expected, the MSPEs for the MS-GJR-MS-vine model with MNoI equal to 200 are smaller compared to lower MNoI values. A higher MNoI allows the algorithm to converge better in terms of the log-likelihood, resulting in parameter estimates closer to the actual parameters. To assess the differences in forecasts, I perform paired t-tests with the null hypothesis of no difference in forecast means for the algorithm with MNoI set to 200. When the MNoI is set to 50, the forecast are significantly different from those with MNoI equal to 200, indicating that log-likelihood convergence is not always achieved. For MNoI equal to 100, only the forecast mean for power differs signficantly under the 10% confidence level from the forecast mean with MNoI equal to 200. This finding suggets that the algorithm mostly converges to the optimal log-likelihood before reaching the MNoI equal to 100. Consequently, I decide to set the MNoI equal to 100 in the rest of the results.

Table 5.1: Breakdown of the mean squared prediction errors of forecasted energy commodities generated by the MS-GJR-MS-vine model per maximum number of iterations in the EM-algorithm.

MNoI	Oil	Gas	Coal	Power
200	1.677	17.350	0.209	1440.972
100	1.680	17.407	0.216	1442.869*
50	1.725***	18.648***	0.381***	1461.342***

Note. The asterisks denote the significance of the paired t-test between the model with 1 update step and one of the other models; * p < 0.10, ** p < 0.05, *** p < 0.01.

After setting the MNoI, one iteration of the rolling window for the MS-GJR-MS-vine model still takes up to 20 hours to either converge or to reach the MNoI. Since the forecasting period is 130 days in length, I aim to further reduce the computation time by updating the MS-GJR-MS-vine model parameters every 5 or 10 iterations of the rolling window, corresponding to one or two weeks, respectively. To assess the effect of this decision, I generate forecasts for the same period (January 1, 2023, until June 30, 2023) for all four energy commodities with different update steps, compute the corresponding MSPEs and perform paired t-tests. The results are shown in Table 5.2. When the parameters are updated every two weeks, the forecasts for oil, gas and power

differ significantly compared to when the parameters are updated every day. In case of updating the parameters every week, only the gas and power forecasts differ signifcantly under the 10% confidence level. This is explained by the fact that gas and power prices are more volatile, making them harder to forecast based on non-recently estimated parameters. However, for each model I choose to update the parameters every 5 iterations of the rolling window to reduce computation time by 5 times and take the loss in accuracy for given. This is justified, as I run the benchmark models with the same configurations.

Table 5.2: Breakdown of the mean squared prediction errors of forecasted energy commodities generated by the MS-GJR-MS-vine model for different update steps.

Update step	Oil	Gas	Coal	Power
1	1.680	17.307	0.216	1442.869
5	1.688	17.459*	0.234	1444.084*
10	1.690*	17.607**	0.234	1450.047***

Note. The asterisks denote the significance of the paired t-test between the model with 1 update step and one of the other models; * p < 0.10, ** p < 0.05, *** p < 0.01.

5.2 Forecasts

As explained in Section 4.2, I generate forecasts over a relatively volatile period spanning from January 3, 2022, until June 30, 2022, and a relatively stable period covering January 1, 2023 until, June 30, 2023, for the GJR-MS-vine, MS-GJR-MS-vine and their benchmark models, and evaluate their performance in terms of the FB, MAE and MSPE. To compare the generated forecasts across the models I again employ the paired t-test. The results are displayed in Tables 5.3 and 5.4 and they provide valuable insights about the forecasting performance of the models.

Table 5.3: The forecast biases, mean absolute errors and mean squared prediction errors of a volatile and a stable period for the models per energy commodity.

	FB				MAE				MSPE			
Model	Oil	Gas	Coal	Power	Oil	Gas	Coal	Power	Oil	Gas	Coal	Power
Volatile period												
MS-GJR-MS-vine	**0.189**^{2}	**0.281**^{2}	**0.139**^{2}	**−0.574**^{2}	**1.211**^{1}	**6.674**^{1}	**0.453**^{2}	**36.836**^{2}	**2.916**^{1}	**155.001**^{2}	**0.804**^{1}	**4466.680**^{2}
GJR-MS-vine	0.225	**−0.262**^{1}	0.142	−1.697	**1.219**^{2}	6.693	0.459	37.050	**2.931**^{2}	155.380	0.818	4486.240
GJR-vine	**0.143**^{1}	−0.328	−0.152	−1.170	1.263	6.702	0.463	37.498	2.951	156.003	0.927	4483.390
MS-GJR	−0.301	−0.701	0.365	−1.785	1.534	7.232	0.950	39.348	3.327	158.826	1.078	5036.768
MS-vine	0.192	0.409	**0.099**^{1}	**0.348**^{1}	1.237	**6.677**^{2}	**0.448**^{1}	**36.691**^{1}	2.975	**154.716**^{1}	**0.806**^{2}	**4451.743**^{1}
Stable period												
MS-GJR-MS-vine	−0.015	**−0.041**^{1}	**0.001**^{2}	**−0.947**^{2}	**1.059**^{1}	**2.795**^{1}	**0.337**^{2}	**26.342**^{1}	**1.688**^{1}	**17.459**^{1}	**0.234**^{2}	**1444.084**^{1}
GJR-MS-vine	**0.009**^{1}	−0.132	**0.000**^{1}	−1.305	**1.060**^{2}	**2.881**^{2}	0.337	26.408	**1.693**^{2}	**17.503**^{2}	**0.233**^{1}	1446.723
GJR-vine	**−0.012**^{2}	−0.118	−0.001	−1.319	1.061	2.888	**0.335**^{1}	26.472	1.695	17.649	0.235	1447.709
MS-GJR	−0.017	**0.048**^{2}	−0.005	−1.286	1.071	2.943	0.351	26.389	1.803	17.735	0.246	1446.027
MS-vine	−0.020	0.051	−0.021	**−0.654**^{1}	1.078	2.894	0.364	**26.364**^{2}	1.850	17.524	0.254	**1445.468**^{2}

Note 1. The (second) best performing value for a specific forecast measure and energy commodity is in bolt and is indexed with (2) 1.

Note 2. The volatile and stable periods correspond to, respectively, January 3, 2022, until June 30, 2022, (129 observations) and January 1, 2023, until June 30, 2023 (130 observations).

First of all, during the stable period, most models show negative FB for the energy commodities. This suggests that the models consistently overforecast the energy commodity prices. This overforecasting tendency can be attributed to the fact that the models are estimated on a period that encompasses periods of high volatility (January 1, 2015, to December 31, 2022), while the forecasting period (January 1, 2023, to June 30, 2023) experienced relatively lower volatility. Consequently, the estimated parameters do not totally reflect to the forecasts and differentiating between a high and low volatility regime becomes evident. For instance, in the case of the one-regime combination of GJR-GARCH and a vine copula (GJR-vine), all energy commodities are overforecasted. However, by introducing a high and low volatility state in the GJR-vine model, adding up to the MS-GJR-MS-vine model, the overforecasting is reduced. The opposite finding can be inferred in the volatile period where the FB is mostly positive, indicating underforecasting. This shows that the models are unable to fully incorporate the large price fluctuations observed during the first half of 2022.

Secondly, in both the volatile and stable periods the largest MAE and MSPE are observed for power. This aligns with Section 3 as the largest price differences are observed for power. Yet, the MS-GJR-MS-vine outperforms the benchmark models in terms of MAE and MSPE for oil, gas and power. This indicates that the model's forecasted energy commodity prices are generally closest to the actual energy prices, even when penalizing the large prediciton errors by squaring them in the MSPE.

Furthermore, during the volatile period, the MS-GJR-MS-vine performs (second) best for all energy prices in terms of both MAE and MSPE, sometimes being outperformed by the MS-vine model. Referring to Table 5.4, it is evident that the forecasted energy prices from both the MS-GJR-MS-vine and MS-vine models do not significantly differ, except for the forecasted oil prices, where the MS-GJR-MS-vine outperforms the MS-vine. Additionally, in the stable period, the MS-GJR-MS-vine model ranks second best in forecasting coal prices and it is outperformed by the GJR-MS-vine model in terms of the FB and MSPE and by the GJR-vine model in terms of MAE. However, these differences are marginal at, respectively, 0.001 and 0.002. Combining this insight with the conclusion that the GJR-vine and GJR-MS-vine coal price forecasts do not devaite significantly from the coal price forecasts generated by the MS-GJR-MS-vine model (Table 5.4), and I conclude that the MS-GJR-MS-vine model overall performs best in both the volatile and stable period.

The fact that the MS-GJR-MS-vine model overall has better forecasting performance than the GJR-MS-vine and the benchmark models highlights the importance of not only modelling regime-switching returns or volatility, but that the residual part of the returns (Equation 4.1) should be considered to be in a high and low volatility state as well. The MS-GJR-MS-vine model

Table 5.4: The significance levels for the paired t-test between the forecasts of the benchmark models and the MS-GJR-MS-vine model over a volatile (January 3, 2022, until June 30, 2022) and stable period (January 1, 2023, until June 30, 2023) with null hypothesis of no differene in forecast means.

	Volatile period				Stable period			
Model	Oil	Gas	Coal	Power	Oil	Gas	Coal	Power
MS-GJR-MS-vine	2.916	155.001	0.804	4466.680	1.688	17.459	0.234	1444.084
GJR-MS-vine	***	***	-	***	***	***	-	***
GJR-vine	-	***	-	***	-	***	-	***
MS-GJR	-	-	-	-	***	*	***	*
MS-vine	-	***	***	***	-	***	*	***

Note: - p < 1.0, * p < 0.10, ** p < 0.05, *** p < 0.01

captures the volatility through a GJR-GARCH volatility model and it models and combines the corresponding standardized residuals by utilizing a vine copula. Introducing regime-switching in modelling the GJR-GARCH volatilities modelling enhances the forecasting ability, aligning with Xiao (2021), who proved that MS GARCH models improves forecasting the extreme risks in energy prices, and Cifter (2013), who showed that MS GARCH enhanced the forecasting ability in the Nordic electric power market. Subsequently, extending Markov-switching to the standardized residuals of the regime-switching GJR-GARCH results in a superior forecasting model.

Figures 5.1a and 5.1b present the probabilities of being in a high volatility state during both a volatile and stable period, as generated by the MS-GJR-MS-vine model. At first sight, power prices seems to be very volatile in both figures. However, Figure 5.1a depicts the power prices ranging from 50 to 700 euros, while Figure 5.1b confines them within the range of 20 to 200 euros. A similar observation can be found for the other energy prices, as they maintain almost constant prices during the stable period in Figure 5.1b, while the volatile period in Figure 5.1a indicates an upward trend. This volatility is marked by frequent high spikes in the probability, indicating more certainty of being in the high volatility state. In contrast, the stable period exhibits less upward spikes and more downward spikes, indicating the energy prices are in the low volatility state. Additionally, the up- or downward spikes in the probability of being in the high volatility state appear to closely follow the fluctuations in the power and gas prices. This relationship may be attributed to the fact that these two energy prices are more volatile and exhibit higher prices compared to coal and oil prices. As a consequence, these energy prices carry greater weights within the EM-algorithm, resulting in state probabilities which are more sensitive to variations in power and gas prices.

5.3 In-sample analysis

For the in-sample analysis of the (benchmark) models, I generate 1,000,000 simulated energy commodity prices from the (benchmark) models. Subsequently, I construct the unhedged P&Ls

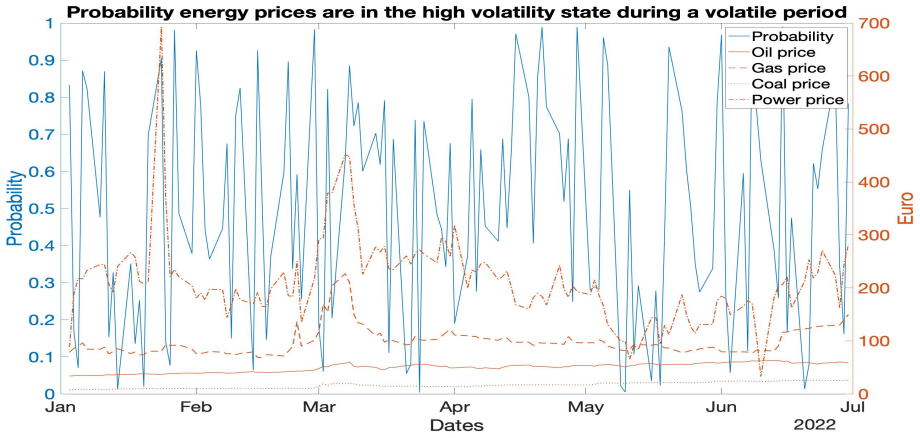

(a)

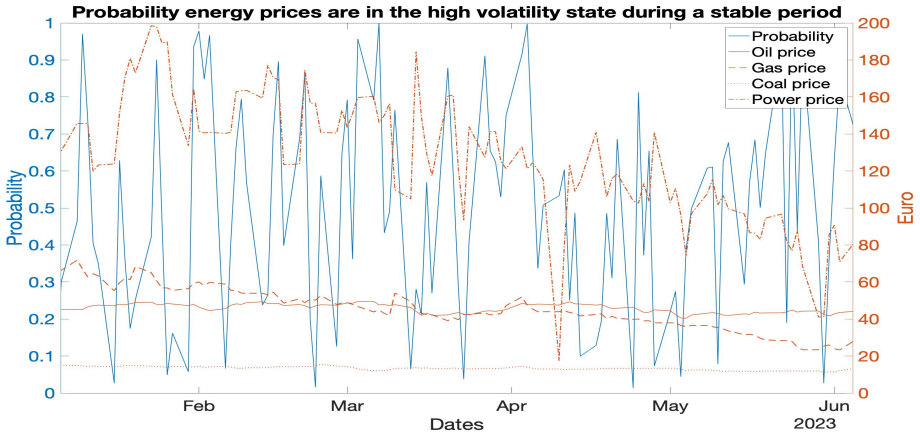

(b)

Figure 5.1: Figures 5.1a and 5.1b illustrate the MS-GJR-MS-vine probabilities whether the four energy prices (oil, gas, coal and power) are in the high volatility state during, respectively, a volatile period spanning from January 3, 2022, until June 30, 2022, and a stable period covering January 1, 2023, until June 30, 2023.

from the simulations based on the underlying assumptions explained in Section 4.3. Each unhedged P&L combination corresponds to the consumption of one MWh of $r_{1,t}$ and one MWh of $r_{2,t}$. These P&Ls remain unhedged, meaning that $b_1 = 0$ and $b_2 = 0$. This in-sample simulation allows for a risk level comparison between the (benchmark) models, which can then be verified with the actual risks at different confidence levels over the period January 1, 2015, to June 30, 2023. If the VaR and ES simulated by a (benchmark) model align with the actual VaR and ES for different confidence levels, it is an indication that the model correctly models the tail of the distribution. The results of the in-sample simulation are displayed in Table 5.5. Here, the VaR or ES that best aligns with the actual VaR and ES of the unhedged P&Ls across the models is highlighted in bolt. As an example, I interpret the VaR and ES at a 90% confidence level for unhedged P&L-1 simulated by the MS-GJR model with, respectively, values 2.316 and 4.845. If an energy consumer holds 1 MWh of oil and gas, than in 10% of the situations, the combined price is at least 2.316 euros higher the following day. On average the price will be 4.845 euros higher the next day. Besides

this interpretation, a few other conclusions can be drawn from Table 5.5.

Table 5.5: The Value-at-Risk and expected shortfall at various confidence levels for P&L-1 to 6 per (benchmark) model.

		Value-at-Risk			Expected shortfall				Value-at-Risk			Expected shortfall		
		90%	95%	99%	90%	95%	99%		90%	95%	99%	90%	95%	99%
Actual	*P&L-1*	1.755	4.227	15.620	7.625	12.717	30.619	*P&L-2*	15.789	31.411	88.467	49.219	76.714	160.204
MS-GJR-MS-vine		2.069	3.566	11.328	5.989	9.312	23.075		14.746	25.479	74.305	42.441	65.859	**164.122**
GJR-MS-vine		2.430	4.800	15.075	**7.525**	11.674	25.937		16.865	**30.347**	**84.398**	**46.614**	**70.882**	164.778
GJR-vine		2.038	4.528	18.337	8.317	**13.678**	**32.908**		17.589	34.258	104.435	55.494	86.726	207.135
MS-GJR		2.316	4.729	**15.430**	4.845	10.019	24.948		17.032	33.031	101.247	57.091	69.053	186.702
MS-vine		**1.758**	**4.028**	13.718	6.675	10.750	25.499		**15.098**	28.278	76.870	42.408	64.820	131.527
Actual	*P&L-3*	15.961	33.543	94.573	51.098	79.627	164.868	*P&L-4*	15.652	31.399	88.597	49.186	76.691	160.109
MS-GJR-MS-vine		15.455	26.317	75.588	43.342	66.890	**165.460**		16.687	28.588	80.635	**46.043**	**70.601**	171.637
GJR-MS-vine		18.819	**32.972**	**88.101**	**49.425**	**74.172**	169.250		16.297	**29.737**	**83.639**	45.944	70.127	**163.796**
GJR-vine		19.413	36.390	106.049	57.386	88.481	208.282		17.555	34.207	104.463	55.459	86.698	88.597
MS-GJR		17.485	34.692	102.896	61.201	74.096	188.364		16.960	32.934	100.818	56.684	68.992	184.003
MS-vine		**15.894**	29.913	80.859	44.202	67.230	137.832		**15.392**	28.965	61.894	37.801	54.519	107.999
Actual	*P&L-5*	0.886	1.320	2.502	1.615	2.145	3.824	*P&L-6*	1.316	4.272	15.454	7.482	12.692	30.451
MS-GJR-MS-vine		0.763	1.054	1.782	1.212	1.530	2.417		**1.310**	2.708	10.377	5.110	8.359	21.956
GJR-MS-vine		0.731	1.019	1.827	1.201	1.545	2.511		1.843	4.271	**14.397**	6.941	11.061	25.110
GJR-vine		**0.883**	**1.270**	**2.383**	**1.521**	**1.991**	**3.329**		1.488	**4.262**	18.169	**8.000**	**13.494**	**32.728**
MS-GJR		0.733	1.109	1.630	1.172	1.502	2.332		1.688	3.290	13.170	6.138	8.093	23.530
MS-vine		0.675	0.950	1.717	1.119	1.443	2.346		1.794	4.083	13.869	6.187	9.616	20.363

Note. The simulated risk for each measure, unhedged P&L combination and confidence interval that is closest to the actual risk across the models is highlighted in bolt.

First of all, the unhedged P&L-2 to 4 show relativley large VaR and ES compared to the other unhedged P&Ls. This finding is primarily due to the fact that these three unhedged P&Ls are build from power, a commodity that experienced significant price fluctuations since the start of the Russo-Ukrainian war. Consequently, power prices were highly volatile during this period, resulting in relatively high positive and low negative returns and explaining the higher VaR and ES. Due to the size of the power return compared to the other energy commodity returns, the unhedged P&L-2 to 4 are dominated by the power returns and, therefore, mostly reflects the risks of buying 1 MWh hour of power.

Furthermore, the GJR-MS-vine model exhibits the best VaR and ES performance for most confidence levels in the case of the unhedged P&L-2 to 4, meaning that the simulated risk measures best align with the actual risks. In the cases where it does not rank first, it still notes the second-best performance. Unhedged P&L-2 to 4 have in common that they are build from power. So, the GJR-MS-vine model best captures the upper-tail risks in buying 1 MWh of power. Moreover, for the unhedged P&L-5 and 6, the GJR-vine model yields the most accurate VaR and ES simulations. Here, the common feature is coal. While coal is also included in unhedged P&L-4, its impact is relatively small due to the dominating power price returns. As a result, the GJR-vine best simulates the risks associated with 1 MWh of coal, unless its combined with 1 MWh of power. In the case of unhedged P&Ls build from at least 1 MWh power, the GJR-MS-vine is recommended.

Lastly, the MS-vine model occassionally outperforms other models in modelling the VaR and

ES, particularly for the 90% confidence level, for unhedged P&L-1 to 4. Additionally, the VaR and ES for other confidence levels are often quite close to the actual values. However, both the MS-GJR-MS-vine and MS-GJR models do not play a significant role in modelling the VaR and ES as their simulated VaR and ES do not align with the actual VaR and ES. This observation suggests that the Markov-switching GJR-GARCH part of these models may not effectively capture the risks in energy price returns and could potentially lead to overfitting. Despite the MS-GJR-MS-vine model performing well in forecasting, it struggles to accurately model the extreme risks associated with holding multiple energy commodities. This may be attributed to the fact that the MS-GJR-MS-vine model sufficiently models the expected behaviour of the energy price distribution, but it falls short in capturing the upper tail distribution.

Nevertheless, the combination of GJR-GARCH and (regime-switching) vine copulas proves to be most effective in modelling VaR and ES, in contrast to the MS-GJR-MS-vine model.

5.4 Out-of-sample hedging

The out-of-sample minimum-VaR and ES HE at various confidence levels for different models are displayed in Table 5.6 with the median in between parentheses and the highest mean per hedging method and confidence interval is highlighted bolt. Besides, the corresponding HR can be found in Tables J.1 and J.2 in Appendix J. Ideally, for a risk-averse energy consumer seeking for hedges that reduce his energy risks accordingly, the mean and median HE should be close to each other. This suggests that the set of HEs is approximately symmetrically distributed and not a lot of extreme positive or negative HE outliers occur. On the other hand, when the mean and median HE are far apart, it indicates that the HE set is skewed. In case the mean is larger (smaller) than the median, more positive (negative) HE outliers are expected. In Table 5.6 both cases are observed. For a visual representation, graphs of the minimum-VaR and ES HE for P&L-1 over the period January 1, 2023, until June 30, 2023, for different confidence levels are shown in, respectively, Figures I.1 and I.2 in Appendix I. Here the aforementioned becomes clear as MS-GJR-MS-vine and MS-vine show large negative peaks in the HE, resulting in a mean way smaller than the median. In the end, this may hinder effective minimum-VaR or ES hedging strategies.

The MS-GJR-MS-vine model is consistently outperformed by the benchmark models in both minimum-VaR and ES out-of-sample hedging. Comparing the means and medians of the out-of-sample HE for P&L-1, 5 and 6 reveals a lot of negative outliers in the HE performance of the MS-GJR-MS-vine model. This indicates that the simulations generated by the MS-GJR-MS-vine model fail to accurately capture the risks in the upcoming month, leading to unrealible hedge ratios. This finding aligns with the conclusion drawn in Section 5.3, where the in-sample analysis

Table 5.6: Average out-of-sample hedge effectiveness corresponding to hedged P&L-1 to 6 with the median in parentheses for various models and confidence intervals.

	Value-at-Risk			Expected Shortfall		
	90%	95%	99%	90%	95%	99%
P&L - 1						
MS-GJR-MS-vine	-69.481(-47.319)	-26.213(- 0.149)	- 6.070(- 0.301)	-14.319(- 3.032)	- 6.839(3.113)	- 7.890(- 1.672)
GJR-MS-vine	- 5.678(- 0.054)	- 0.579(0.054)	-10.094(- 1.325)	2.069(6.270)	0.783(7.421)	-11.301(- 4.701)
GJR-vine	**0.372(0.032)**	**1.592(0.045)**	- 3.062(0.284)	**6.485(7.764)**	**7.012(8.610)**	**4.568(- 0.376)**
MS-GJR	- 1.207(- 2.004)	0.516(- 1.869)	**- 0.209(- 1.301)**	-21.510(-10.973)	-21.526(-23.330)	-21.510(-10.973)
MS-vine	-27.329(- 0.005)	-24.756(0.929)	-67.101(- 0.004)	-62.439(0.761)	-66.679(1.250)	-83.515(0.532)
P&L - 2						
MS-GJR-MS-vine	- 3.889(- 3.084)	- 1.040(0.040)	- 1.653(- 2.786)	- 1.988(- 1.656)	- 1.372(- 0.820)	- 1.661(- 2.984)
GJR-MS-vine	- 0.923(- 0.015)	**1.534(0.116)**	**1.694(1.087)**	0.747(0.122)	1.983(0.698)	**1.989(2.196)**
GJR-vine	**- 0.067(- 0.006)**	0.120(0.006)	- 0.335(- 0.218)	- 0.159(- 0.149)	- 0.118(- 0.150)	- 0.382(- 0.692)
MS-GJR	- 2.397(- 5.817)	- 1.251(- 0.990)	- 3.877(- 3.530)	0.128(- 0.092)	- 2.084(- 0.825)	- 3.961(- 2.574)
MS-vine	- 6.199(- 0.557)	- 0.149(0.194)	- 8.911(- 1.595)	**3.238(7.090)**	**3.875(8.389)**	- 4.972(- 3.148)
P&L - 3						
MS-GJR-MS-vine	**0.984(0.120)**	0.238(0.364)	0.204(- 0.981)	0.562(0.310)	0.194(- 0.511)	- 0.225(- 0.467)
GJR-MS-vine	- 1.118(0.004)	**1.275(- 0.003)**	**1.760(- 0.007)**	**2.997(0.120)**	**4.173(1.783)**	**4.097(0.066)**
GJR-vine	0.143(0.028)	0.031(0.023)	- 0.181(- 0.113)	0.335(0.163)	0.111(- 0.029)	- 0.449(- 1.024)
MS-GJR	- 0.801(- 1.271)	0.624(0.071)	0.031(- 0.109)	0.006(- 1.239)	- 0.295(- 1.093)	- 0.519(- 2.308)
MS-vine	0.443(0.427)	0.512(0.336)	0.037(0.174)	0.530(0.664)	0.327(0.098)	- 0.137(- 1.024)
P&L - 4						
MS-GJR-MS-vine	0.103(- 0.057)	- 0.561(- 0.827)	**0.417(- 1.423)**	0.936(- 0.104)	0.693(0.207)	0.261(- 0.779)
GJR-MS-vine	**0.950(0.014)**	**0.601(0.065)**	0.366(- 0.065)	**1.228(- 0.567)**	**1.177(- 0.502)**	**1.613(- 0.856)**
GJR-vine	0.020(- 0.031)	- 0.015(0.022)	- 0.135(0.022)	- 0.144(- 0.009)	- 0.192(- 0.010)	- 1.136(- 0.743)
MS-GJR	- 4.391(- 0.748)	- 3.071(- 1.944)	- 1.270(- 0.616)	- 2.508(- 2.401)	- 1.745(- 3.209)	- 1.772(- 1.299)
MS-vine	- 2.796(- 0.080)	- 0.637(- 0.191)	- 1.826(- 0.333)	- 1.875(- 1.219)	- 1.342(- 0.342)	- 1.711(- 0.191)
P&L - 5						
MS-GJR-MS-vine	-29.617(- 7.243)	-18.284(- 1.202)	- 1.955(- 0.290)	1.003(- 0.476)	1.504(3.073)	1.993(3.601)
GJR-MS-vine	- 1.499(- 0.759)	- 1.834(- 0.450)	0.164(0.142)	**2.515(1.579)**	**1.921(2.584)**	**2.268(6.156)**
GJR-vine	**0.096(- 0.010)**	**0.014(- 0.009)**	**0.754(0.406)**	1.306(1.243)	1.213(1.271)	1.828(2.836)
MS-GJR	-15.662(- 7.108)	-16.925(-10.635)	- 8.951(- 4.427)	-20.081(- 0.875)	-43.503(- 4.103)	-14.203(- 4.807)
MS-vine	- 6.383(0.033)	-24.555(1.192)	-79.586(0.075)	-73.165(2.274)	-82.072(- 0.003)	-105.557(- 0.123)
P&L - 6						
MS-GJR-MS-vine	-43.871(- 1.863)	-22.070(- 0.392)	- 5.996(- 0.120)	-23.405(-10.006)	**- 3.947(- 2.314)**	**- 9.092(- 2.350)**
GJR-MS-vine	-25.852(- 2.994)	-85.513(- 0.138)	-86.909(- 0.407)	-42.220(-11.293)	-30.816(- 3.042)	-30.148(- 4.548)
GJR-vine	- 6.161(0.000)	-10.735(0.027)	**- 0.937(0.437)**	**- 1.639(0.890)**	- 4.706(1.697)	-16.397(1.082)
MS-GJR	-25.403(- 4.575)	-42.034(-10.857)	-47.707(0.302)	-17.843(- 2.502)	-10.572(- 9.803)	-55.290(-15.372)
MS-vine	**- 5.377(- 0.316)**	**- 3.595(- 0.187)**	- 8.674(- 1.476)	- 8.245(- 2.524)	- 6.625(- 0.403)	-10.663(- 2.327)

Note. The average out-of-sample hedge effectiveness for each risk measure, unhedged P&L combination and confidence interval that is highest across the models is highlighted in bolt.

also revealed that the MS-GJR-MS-vine inadequately models the risks in energy commodity price returns. Overall, the MS-GJR-MS-vine model is incapable of providing accurate simulations in the context of energy commodity prices. As a result, energy portfolio risks are incorrectly modelled and leading to the conclusion that the MS-GJR-MS-vine model is not suitable for multiproduct hedging of energy commodities.

However, some of the benchmark models do show promising results in terms of out-of-sample HE. Consequently, based on P&L-1 to 6 and the information provided in Tables 5.5, 5.6, J.1 and J.2, I offer recommendations on whether and how an energy consumer should utilize mutual, multiproduct hedging to reduce his risks in certain energy portfolios by considering all sixs P&Ls.

P&L-1 comprises the hedging of 1 MWh of oil and gas with 1 MWh of coal and power. According to Table 5.5, the GJR-vine model accurately models the ES. Furthermore, implementing

minimum-ES hedging with simulations from the GJR-vine model results in a positive HE, meaning a decrease in ES of at least 4% for all three confidence levels (see Table 5.6). For successfull minimum-ES hedging of 1 MWh oil and gas, Table J.2 suggests hedging these energy commodities by 0.611 to 0.862 MWh of coal and and 0.03 to 0.021 MWh power. In that case an energy consumer decreases his ES with at least 4%. Likewise, minimum-VaR hedging renders a positive HE for the 90% and 95% confidence levels, but Table 5.5 shows that the in-sample VaR does not match the actual VaR. Therefore, I advise against minimum-VaR hedging for P&L-1.

P&L-2, 3 and 4 represent the different hedging combinations of power together with one of the other three energy commodities, namely, oil, gas and coal, hedged with the remaining energy commodities. Table 5.6 shows that the GJR-MS-vine model renders positive HE for minimum-VaR, except at the 90% confidence level, and for minimum-ES hedging. These results are consistent with the findings in Table 5.5, which stated that the GJR-MS-vine model accurately models the in-sample VaR and ES for the hedging combinations involving power. For all three P&L combinations, the percentage risk reduction is largest with minimum-ES hedging. In the case of P&L-4, I observe a positive HE mean and a close to zero or even negative HE median in both minimum-VaR and minimum-ES hedging. This indicates there are some positive outliers in the dataset. Nonetheless, to offer specific multiproduct hedging combinations, the following HR should be considered depending on the energy consumer's objective and energy portfolio. For reducing the VaR:

- P&L-2: Hedge 1 MWh of power and oil with 0.272 to 0.548 MWh of coal and 0.290 to 0.618 MWh of gas to reduce the VaR with -0.923% to 1.694%.
- P&L-3: Hedge 1 MWh of power and gas with 0.320 to 0.451 MWh of coal and 0.310 to 0.377 MWh of oil to reduce the VaR with -1.118% to 1.760%.
- P&L-4: Hedge 1 MWh of power and coal with 0.181 to 0.355 MWh of oil and 0.079 to 0.456 MWh of gas to reduce the VaR with 0.366% to 0.950%.

If the energy consumer rather reduces his ES, he should keep these HR:

- P&L-2: Hedge 1 MWh of power and oil with 0.997 to 1 MWh of coal and 0.953 to 1 MWh of gas to reduce the ES with 0.747% to 1.989%.
- P&L-3: Hedge 1 MWh of power and gas with 0.660 to 0.695 MWh of coal and 0.630 to 0.686 MWh of oil the ES with 2.997% to 4.997%.
- P&L-4: Hedge 1 MWh of power and coal with 0.572 to 0.652 MWh of oil and 0.829 to 0.903 MWh of gas the ES with 1.177% to 1.613%.

When hedging 1 MWh of oil and coal with power and gas (P&L-5), Table 5.6 shows that for minimum-VaR hedging the GJR-vine model is the only model that yields a positive HE. For minimum-ES hedging the MS-GJR-MS-vine and GJR-MS-vine models could also be considered, as they result in higher reductions of the ES. However, based on Table 5.5 the GJR-vine model renders the most accurate VaR and ES across all considered confidence levels. Consequently, I recommend basing the hedge ratios on the simulations generated by the GJR-vine model. For minimum-VaR hedging, the most effective reduction in VaR is achieved when hedging with 0.001 MWh of power and 0.001 to 0.006 MWh of gas (Table J.1). In case of minimum-ES hedging, I recommend to hedge 1 MWh of oil and coal with 0.001 MWh of power and 0.018 to 0.031 MWh of gas (Table J.2).

If the energy consumer intends to hedge 1 MWh of gas and coal with power and oil, I recommend against it, as none of the models can generate accurate hedge ratios that effectively reduce the VaR or ES when holding 1 MWh of gas and coal (see Table 5.6).

Summarizing, the MS-GJR-MS-vine model inadequately models energy prices. As a result, it can not be employed in multiproduct hedging. In contrast, the GJR-MS-vine and benchmark GJR-vine model do effectively model the four energy commodity prices, making them suitable for multiproduct hedging of different hedge combinations. For every pair of energy commodities, except for gas and coal, a multiproduct hedge that reduces the VaR and / or ES can be found. Depending on the hedge and energy commodity pair, the VaR or ES can be reduced up to 7%.

Chapter 6

Conclusion & Discussion

In this paper, I build upon the work of Basetti et al. (2018), who modelled energy prices with an AR-GARCH model and the corresponding dependence structure through a vine copula. I introduce two enhancements to this model. Firstly, I replace the AR-GARCH volatilities with a more suitable GJR-GARCH volatility model to capture the typical characteristics and leverage effect possessed by energy commodities. Additionally, I incorporate regime-dependent dynamics by implementing Markov-switching in the combined GJR-GARCH and vine copula model to include

the regime switches often observed in energy commodity prices, resulting in the novel MS-GJR-MS-vine model. Moreover, I propose a derivative of the MS-GJR-MS-vine model, which again employs the combination of GJR-GARCH volatilities and standardized residuals connected through a vine copula. However, Markov-switching is only incorporated for the standardized residuals, resulting in the GJR-MS-vine model. Due to the large number of parameters, maximum likelihood estimation is not feasible. To overcome this, I improve the stepwise EM-algorithm proposed by Stöber & Czado (2014) by incorporating GJR-GARCH volatilities and integrating the log-likelihood evaluation technique developed by Aas et al. (2009). After estimating the GJR-MS-vine and MS-GJR-MS-vine models, I evaluate their performance in three ways on a dataset consisting of oil, gas, coal and power prices for the period of January 1, 2015, to June 30, 2023. Firstly, I assess their forecasting performance and compare it to other existing models. Secondly, I check the ability of the models in correctly modelling the risks in terms of VaR and ES in an in-sample analysis. And, lastly, I extend the multiproduct futures hedging model proposed by Sukcharoen & Leatham (2017) to four variables and modify it such that it allows for mutual hedging, after which I employ the resulting multiproduct hedging model.

The forecasting analysis shows that the MS-GJR-MS-vine model outperforms its benchmark models and the GJR-MS-vine model in terms of forecast bias, mean absolute error and mean squared prediction error for most energy commodities, highlighting the importance of jointly modelling regime-switching volatility and standardized residuals of the energy returns. Although the GJR-MS-vine model also outperforms its benchmark models in a period with stable energy prices, it does not outperform the MS-GJR-MS-vine model. Further, for the in-sample risk analysis the benchmark model with a one-regime combination of volatility and standardized residuals (GJR-vine) and the GJR-MS-vine model best model the risks in terms of value-at-risk and expected shortfall for, respectively, the coal and power unhedged profit and loss equations. The models with regime-switching volatilities, like the MS-GJR-MS-vine model, do not perform well, suggesting that the Markov-switching GJR-GARCH part of these models may not effectively capture the extreme risks in energy price returns. Out-of-sample, multiproduct hedging shows the practical usefulness of the models for energy consumers. The MS-GJR-MS-vine model inaccurately models energy portfolio risks and it is consistently outperformed by benchmark models in reducing the risks through hedging. Therefore, the MS-GJR-MS-vine model is not practically applicable for energy consumers. However, the GJR-MS-vine and GJR-vine model do effectively model the four energy commodity prices and cover most of the various hedge combinations to reduce the risks in terms of value-at-risk and expected shortfall. By utilizing these methods, an energy consumer can achieve up to a 7% reduction in value-at-risk or expected shortfall.

During my research, I encountered limitations in time and computational power, especially while estimating the Markov-switching GJR-GARCH, which is very time-consuming. Therefore, I am not able to let the stepwise EM-algorithm fully converges to its optimal log-likelihood, update the model every day in making one-step-ahead forecasts and to evaluate the forecast performance with a smaller rolling window, a larger sample size or complementary samples. Further research could try to resolve these problems when more computational power is available. Moreover, further research should consider the costs of developing the program, investing in better computers and the time involved in running the program before implementation. This cost-benefit analysis will help determine whether the benefits from calculating and implementing hedges outweigh the costs. Besides, from a more practical standpoint, transaction costs of buying and selling energy commodities should be taken into account to provide a more realistic representation of the actual trading scenario, as transaction costs directly impact the profitability of the hedging strategies. Moreover, in forecasting the volatile and stable periods I have used different lengths for the estimation windows, making the performance measures uncomparable between the two periods. Further research should investigate whether the MS-GJR-MS-vine model performs better in a period with volatile or stable energy prices. Furthermore, I investigate whether energy commodities can be hedged mutually in the multiproduct hedging model. However, instead of hedging mutually the energy commodities could be hedged with their futures as Sukcharoen & Leatham (2017) intended the multiproduct futures hedging model. A last recommendation for further research involves the energy transition. Given the ongoing global energy transition towards sustainable and renewable energy sources, future research could, for example, employ the successful (benchmark) models in quantifying the risks incurred from the energy transition from electricity obtained from fossil fuels to more sustainable energy sources, like electricity generated from nuclear, hydro and solar generating plants.

Bibliography

Aas, K., Czado, C., Frigessi, A. & Bakken, H. (2009). Pair-copula constructions of multiple dependence. *Insurance: Mathematics and Economics 44*(2), 182-198.

Agora Energiewende & Ember. (2021). The European power sector in 2020: Up-to-date analysis on the electricity transition. Retrieved April 4, 2023, from https://static.agora-energiewende.de/fileadmin/Projekte/2021/2020_01_EU-Annual-Review_2020/A-EW_202_Rep
ort_European-Power-Sector-2020.pdf

Ahmad, W., Sadorsky, P. & Sharma, A. (2018). Optimal hedge ratios for clean energy equities. *Economic Modelling 72*(1), 278-295.

Ahmed, S., Hasan, M.M. & Kamal, M.R. (2022). Russia-Ukraine crisis: The effects on the European stock market. *European Financial Management.*

Aloui, R. & Aïssa, M.S.B. (2016). Relationship between oil, stock prices and exchange rates: A vine copula based GARCH method. *The North American Journal of Economics and Finance 37*(1), 458-471.

Artzner, P., Delbaen, F., Eber, J.-M. & Heath, D. (1999). Coherent measures of risk. *Mathematical Finance 9*(3), 203-228.

Baillie. R.T., Bollerslev, T. & Mikkelsen, H.O. (1996). Fractionally integrated generalized autoregressive conditional heteroskedasticity. *Journal of Econometrics 74*(1), 3-30.

Basetti, F., De Giuli, M.E., Nicolino, E. & Tarantola, C. (2018). Multivariate dependence analysis via tree copula models: An application to one-year forward energy contracts. *European Journal of Operational Research 269*(3), 1107-1121.

Bedford, T. & Cooke, R.M. (2001). Probability density decomposition for conditionally dependent random variables modeled by vines. *Annals of Mathematics and Artificial Intelligence, 32*(1), 245-268.

Bedford, T. & Cooke, R.M. (2002). Vines–a new graphical model for dependent random variables. *The Annals of Statistics 30*(4), 1031-1068.

Bollerslev, T. (1986). Generalized autoregressive conditional heteroskedasticity. *Journal of Econometrics 31*(3), 307-327.

Boomsma, A. (1985). Nonconvergence, improper solutions, and starting values in lisrel maximum likelihood estimation. *Psychometrika 50*(1), 229-242.

Chan, K.F. & Gray, P. (2006). Using extreme value theory to measure Value-at-Risk for daily electricity spot prices. *International Journal of Forecasting 22*(2), 283-300.

Charles, A. & Darné, O. (2019). The accuracy of asymmetric GARCH model estimation. *International Economics 157*(1), 179-202.

Cheong, C.W. (2009). Modeling and forecasting crude oil markets using ARCH-type models. *Energy Policy 37*(6). 2346-2355.

Cifter, A. (2013). Forecasting electricity price volatility with the Markov-switching GARCH model: Evidence from the Nordic electric power market. *Electric Power Systems Research 102*(1), 61-67.

Chollete, L., Heinen, A. & Valdesogo, A. (2009). Modeling international financial returns with a multivariate regime-switching copula. *Journal of Financial Econometrics 7*(4), 437-480.

Clayton, D.G. (1978). A model for association in bivariate life tables and its application in epidemiological studies of familial tendency in chronic disease incidence. *Biometrika 65*(1), 141-151.

Danaher, P.J. & Smith, M.S. (2010). Modeling multivariate distributions using copulas: applications in marketing. *Marketing Science 30*(1), 4-21.

Ding, Z., Granger, C.W.J. & Engle, R.F. (1993). A long memory property of stock market returns and a new model. *Journal of Empirical Finance 1*(1), 83-106.

Eurostat. (2022). Energy statistics - an overview. Retrieved March 30, 2023, from https://ec. europa.eu/eurostat/statistics-explained/index.php?title=Energy_statistics_-_an_overview#::
text=An%20analysis%20of%20the%20final,%25)%20(Figure%2010).

Eurostat. (2022). From where do we import energy? Retrieved February 14, 2023, from https://ec.europa.eu/eurostat/cache/infographs/energy/bloc-2c.html

Fanone, E., Gamba, A. & Prokopczuk, M. (2013). The case of negative day-ahead electricity prices. *Energy Economics 35*(1), 22-34.

Grégoire, V., Genest, C. & Gendron, M. (2008). Using copulas to model price dependence in energy markets. *Energy risk, 5*(5), 58-64.

Fink, H., Klimova, Y., Czado, C. & Stöber, J. (2017). Regime switching vine copula models for global equity and volatility indices. *Econometrics 5*(1), 3.

Fisher, M., Köck, C., Schlüter, S. & Weigert, F. (2009). An empirical analysis of multivariate copula models. *Quantitative Finance 9*(7), 839-854.

Frydenberg, S., Onochie, J.I., Westgaard, S., Midtsund, N. & Ueland, H. (2014). Long-term relationships between electricity and oil, gas and coal future prices - evidence from Nordic countries, Continental Europe and the United Kingdom.

Ghorbel, A. & Trabelsi, A. (2014). Energy portfolio risk management using time-varying extreme value copula methods. *Economic Modelling 38*(1), 470-485.

Glosten, L.R., Jagannathan, R. & Runkle, D.E. (1993). On the relation between the expected value and the volatility of the nominal excess return on stocks. *The Journal of Finance 48*(5), 1779-1801.

Gumbel, E.J. (1960). Bivariate exponential distributions. *Journal of the American Statistical Association 55*(292), 698-707.

Hamilton, J.D. (1988). Rational-expectations econometric analysis of changes in regime: an investigatino of the term structure of interest rates. *Journal of Economic Dynamics and Control 12*(2-3), 385-423.

Hamilton, J.D. (1989). A new approach to the economic analysis of nonstationary time series and the business cycle. *Econometrica 57*(2), 357-384.

Hammoudeh, S., Nguyen, D.K. & Sousa, R.M. (2014). Energy prices and CO_2 emission allowance prices: A quantile regression approach. *Energy Policy 70*(1), 201-206.

Harris, R.D.F. & Shen, J. (2006). Hedging and value at risk. *Journal of Futures Markets 26*(4), 369-390.

Hung, J.C., Wang, Y.H., Chang, M.C., Shih, K.H. & Kao, H.H. (2011). Minimum variance hedging with bivariate regime-switching model for WTI crude oil. *Energy 36*(5), 3050-3057.

Jacobsen, B. & Dannenburg, D. (2003). Volatility clustering in monthly stock returns. *Journal of Empirical Finance 10*(4), 479-503.

Kim, D., Kim. J., Liao, S. & Jung, Y. (2013). Mixture of D-vine copulas for modeling dependence. *Computational Statistics & Data Analysis 64*(1), 1-19.

Kotek, P., Tóth, B.T. & Mezösi, A. (2018). What caused the 2018 March price spikes on TTF? *REKK Policy Brief* (2), 1-4.

Kuik, F., Adolfsen, J.F., Lis, E.M. & Meyler, A. (2022). Energy price developments in and out of the COVID-19 pandemic - from commodity prices to consumer prices. *ECB Economic Bulletin* (4), 13-25.

Laporta, A.G., Merlo, L. & Petrella, L. (2018). Selection of Value at Risk models for energy commodities. *Energy Economics 74*(1), 628-643.

Lee, H. & Lee, C. (2022). A regime-switching real-time copula GARCH model for optimal futures hedging. *International Review of Financial Analysis 84*

Linsmeier, T.J. & Pearson, N.D. (2000). Value at Risk. *Financial Analysts Journal 56*(2), 47-67.

Lu, X.F., Lai, K.K. & Liang, L. (2014). Portfolio value-at-risk estimation in energy futures markets with time-varying copula-GARCH model. *Annals of Operations Research 219*(1), 333-357.

Marimoutou, V., Raggad, B. & Trabelsi, A. (2009). Extreme value theory and Value at Risk: Application to oil market. *Energy Economics 31*(4), 519-530.

Nelsen, R.B. (1999) An introduction to copulas. New York: Springer-Verlag.

Nerlinger, M. & Utz, S. (2022). The impact of the Russia-Ukraine conflict on energy firms: A capital market perspective. *Finance Research Letters 50*.

Nugroho, D.B., Kurniawati, D., Panjaitan, L.P., Kholil, Z., Susanto, B. & Sasongko, L.R. (2019). Empirical performance of GARCH, GARCH-M, GJR-GARCH and log-GARCH models for returns volatility. *Journal of Physics 1307*, 52-60.

Sokhanvar, A. & Bouri, E. (2022). Commodity price shocks related to the war in Ukraine and exchange rates of commodity exporters and importers. *Borsa Istanbul Review 23*(1), 44-54.

Sklar, A. (1959). Fonctions de répartition à n dimensionset leurs marges. *Publications de l'Institut de Statistique de l'Université de Paris 8*(1), 229-231.

Smetanina, E. (2017). Real-time GARCH. *Journal of Financial Econometrics 15*(4), 561-601.

Suenaga, H. & Smith, A. (2011). Volatility dynamics and seasonality in energy prices: implications for crack-spread price risk. *The Energy Journal 32*(3).

Sukcharoen, K. & Leatham, D.J. (2017). Hedging downside risk of oil refineries: A vine copula approach. *Energy Economics 66*, 493-507.

Stern, D.I. (2000). A multivariate cointegration analysis of the role of energy in the US macroeconomy. *Energy Economics 22*(2), 267-283.

Stern, D.I. (2011). The role of energy in economic growth. *Ecological Economics Reviews 1219*(1), 26-51.

Stöber, J. & Czado, C. (2014). Regime switches in the dependence structure of multideminsional financial data. *Computational Statistics & Data Analysis 76*(1), 672-686.

Tasche, D. (2002). Expected shortfall and beyond. *Journal of Banking & Finance 26*(1), 1519-1533.

Tayefi, M. & Ramanathan, T.V. (2016). An overview of FIGARCH and related time series models. *Austrian Journal of Statistics 41*(3), 175-196.

Timmerman, A. (2000). Moments of Markov switching models. *Journal of Econometrics 96*(1), 75-111.

Tse, Y.K. (1998). The conditional heteroskedasticity of the yen-dollar exchange rate. *Journal of Applied Econometrics 13*(1), 49-55.

Tseng, J.J. & Li, S.P. (2012). Quantifying volatility clustering in financial time series. *International Review of Financial Analysis 23*, 11-19.

US Department of Energy (2020). Biomass to biofuels: glossary of terms and conversion factors. In Dahiya, A. (Ed.), *Bioenergy: Biomass to Biofuels and Waste to Energy* (pp. 51-63). Cambridge, Massachusetts: Academic Press.

Wang, Y. & Wu, C. (2012). Forecasting energy market volatility using GARCH models: Can multivariate models beat univariate models? *Energy Economics 34*(6), 2167-2181.

Wang, Y., Geng, Q. & Meng, F. (2019). Futures hedging in crude oil markets: A comparison between minimum-variance and minimum-risk frameworks. *Energy 181*(1), 815-826.

Wu, C.F.J. (1983). On the convergence properties of the EM algorithm. *The Annals of Statistics 11*(1), 95-103.

Xiao, Y. (2020). Forecasting extreme risk using regime-switching GARCH models: a case from an energy commodity. *International Journal of Emerging Markets 16*(8), 1556-1582.

Yagi, M. & Managi, S. (2023). The spillover effects of rising energy prices following 2022 Russian invasion of Ukraine. *Economic Analysis and Policy 77*(1), 680-695.

Yang, S.R. & Brorsen, B.W. (1992). Nonlinear dynamics of daily cash prices. *American Journal of Agricultural Economics 74*(3), 706-715.

Zheng, X. (2015). Culture, Investment behaviour and stock market volatility A Markov regime-switching GJR-GARCH approach. *Global Review of Accounting and Finance 6*(2), 56-81.

Appendix A

Descriptive statistics daily energy commodity spot prices

As advocated in Section 1, energy commodity prices exhibit some typical characteristics. Energy commodity prices are characterized by high volatility, high correlations and seasonality which differentiate them from other types of financial data. Consequently, energy commodity prices require special attention in modelling. In this section I demonstrate that the employed dataset also exhibits the three aforementioned characteristics. First of all, energy commodities are very volatile. This is supported by Table A.1, which shows high standard deviations, low minima and high maxima for the energy commodities. The price of power even reached an ultime high at 9 September 2021 when one MWh was sold for 911.35 EUR.

Table A.1: Descriptive statistics of the energy commodity spot prices (in EUR) over the period January 1, 2015, until June 30, 2023.

	Sample size	Mean	St. Dev.	Min.	Max.	Skewness	Kurtosis
Oil	2217	31.087	10.744	9.180	63.034	0.921	0.512
Gas	2217	34.023	41.229	3.100	330.000	2.933	9.950
Coal	2217	6.652	5.580	2.870	28.753	2.222	4.188
Power	2217	87.644	81.212	6.135	911.347	3.050	12.968

Secondly, energy commodities are highly correlated. As depicted in Table A.2, the correlations between the energy commodity prices are at least 0.631. This gives a good reason to model the energy commodity prices jointly.

Table A.2: Correlations between the energy commodity spot prices over the period January 1, 2015, until June 30, 2023.

	Oil	Gas	Coal	Power
Oil	1.000	0.725	0.862	0.631
Gas	0.725	1.000	0.865	0.900
Coal	0.862	0.865	1.000	0.746
Power	0.631	0.900	0.746	1.000

And, lastly, energy commodity prices are prone to seasonality. Figures A.1a - A.1d substantiate this statement, as it is clear that significant negative autocorrelations return at around 500 lags and 1600 lags. In the case of oil spot prices there are also significant positive autocorrelations observed at 1000 lags.

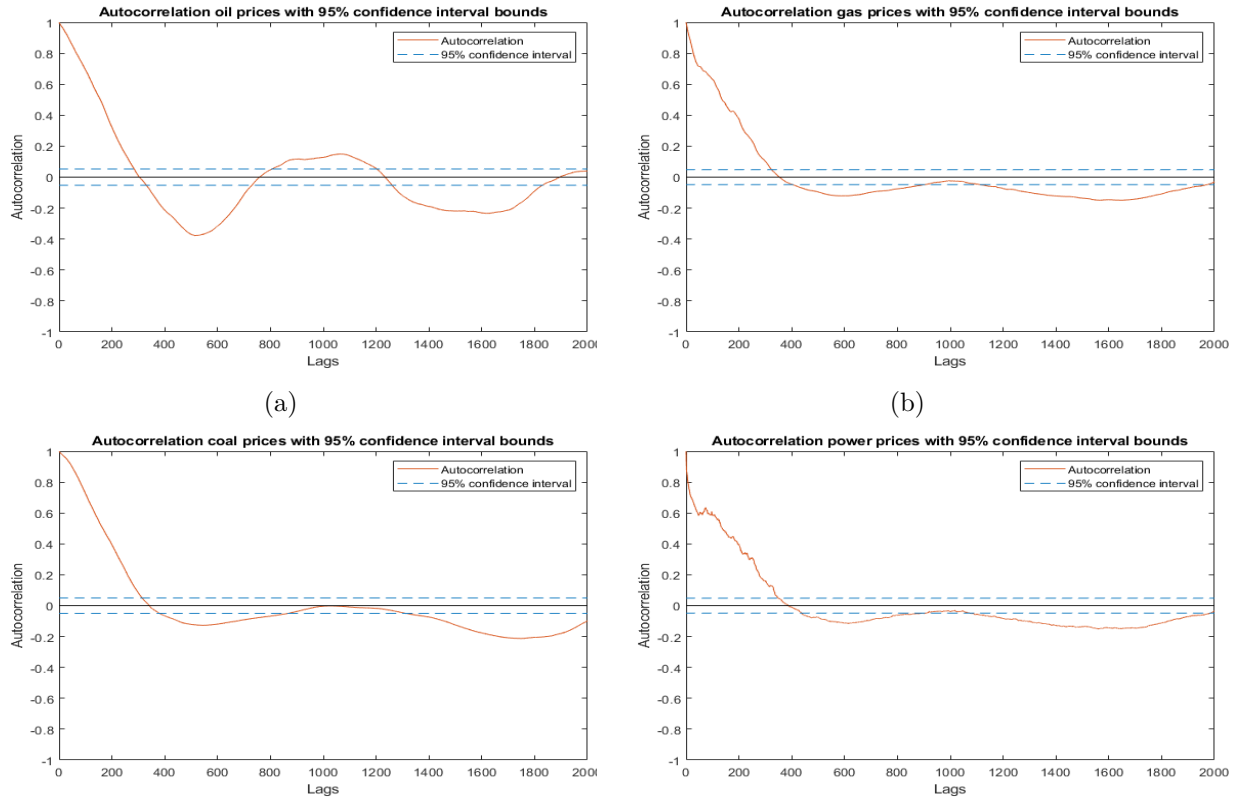

Figure A.1: Graphs with the autocorrelations of the four energy commodities oil A.1a, gas A.1b, coal A.1c and power A.1d and the corresponding 95% confidence intervals over the sample period January 1, 2015, until June 30, 2023.

Appendix B

Derivation conditional pdf's vine copulas

B.1 C-vine copula

$$
\begin{aligned}
f(r_1, r_2, r_3, r_4|\mathcal{F}_t) &= f_{3,4|1,2}(r_3, r_4|r_1, r_2, \mathcal{F}_t) \cdot f_{1,2}(r_1, r_2|\mathcal{F}_t) \\
&= c_{3,4|1,2}(u_{3|1,2}, u_{4|1,2}|\mathcal{F}_t) \cdot f_{3|1,2}(r_3|r_1, r_2, \mathcal{F}_t) \cdot f_{4|1,2}(r_4|r_1, r_2, \mathcal{F}_t) \cdot f_{1,2}(r_1, r_2|\mathcal{F}_t) \\
&= c_{3,4|1,2}(u_{3|1,2}, u_{4|1,2}|\mathcal{F}_t) \cdot \frac{f_{2,3|1}(r_2, r_3|r_1, \mathcal{F}_t)}{f_{2|1}(r_2|r_1, \mathcal{F}_t)} \cdot \frac{f_{2,4|1}(r_2, r_4|r_1, \mathcal{F}_t)}{f_{2|1}(r_2|r_1, \mathcal{F}_t)} \cdot f_{1,2}(r_1, r_2|\mathcal{F}_t) \\
&= c_{3,4|1,2}(u_{3|1,2}, u_{4|1,2}|\mathcal{F}_t) \cdot c_{2,3|1}(u_{2|1}, u_{3|1}|\mathcal{F}_t) \cdot f_{3|1}(r_3|r_1, \mathcal{F}_t) \cdot c_{2,4|1}(u_{2|1}, u_{4|1}|\mathcal{F}_t) \\
&\times f_{4|1}(r_4|r_1, \mathcal{F}_t) \cdot f_{1,2}(r_1, r_2|\mathcal{F}_t) \\
&= c_{3,4|1,2}(u_{3|1,2}, u_{4|1,2}|\mathcal{F}_t) \cdot c_{2,3|1}(u_{2|1}, u_{3|1}|\mathcal{F}_t) \cdot \frac{f_{1,3}(r_1, r_3|\mathcal{F}_t)}{f_1(r_1|\mathcal{F}_t)} \cdot c_{2,4|1}(u_{2|1}, u_{4|1}|\mathcal{F}_t) \\
&\times \frac{f_{1,4}(r_1, r_4|\mathcal{F}_t)}{f_1(r_1|\mathcal{F}_t)} \cdot f_{1,2}(r_1, r_2|\mathcal{F}_t) \\
&= c_{3,4|1,2}(u_{3|1,2}, u_{4|1,2}|\mathcal{F}_t) \cdot c_{2,3|1}(u_{2|1}, u_{3|1}|\mathcal{F}_t) \cdot c_{1,3}(u_1, u_3|\mathcal{F}_t) \cdot f_3(r_3|\mathcal{F}_t) \\
&\times c_{2,4|1}(u_{2|1}, u_{4|1}|\mathcal{F}_t) \cdot c_{1,4}(u_1, u_4|\mathcal{F}_t) \cdot f_4(r_4|\mathcal{F}_t) \cdot f_{1,2}(r_1, r_2|\mathcal{F}_t) \\
&= c_{3,4|1,2}(u_{3|1,2}, u_{4|1,2}|\mathcal{F}_t) \cdot c_{2,3|1}(u_{2|1}, u_{3|1}|\mathcal{F}_t) \cdot c_{1,3}(u_1, u_3|\mathcal{F}_t) \cdot f_3(r_3|\mathcal{F}_t) \\
&\times c_{2,4|1}(u_{2|1}, u_{4|1}|\mathcal{F}_t) \cdot c_{1,4}(u_1, u_4|\mathcal{F}_t) \cdot f_4(r_4|\mathcal{F}_t) \cdot c_{1,2}(u_1, u_2|\mathcal{F}_t) \cdot f_1(r_1|\mathcal{F}_t) \cdot f_2(r_2|\mathcal{F}_t), \\
&= c_{1,2,3,4}(u_1, u_2, u_3, u_4|\mathcal{F}_t),
\end{aligned}
$$

where $u_i = F_i(r_i|\mathcal{F}_t)$ and $u_{i|j} = F_{i|j}(r_i|r_j, \mathcal{F}_t)$ with $i = 1, \ldots, 4; i \neq j$. Reordering the terms such that the most basic functions are in the front, gives

$$
\begin{aligned}
f(r_1, r_2, r_3, r_4|\mathcal{F}_t) &= f_1(r_1|\mathcal{F}_t) \cdot f_2(r_2|\mathcal{F}_t) \cdot f_3(r_3|\mathcal{F}_t) \cdot f_4(r_4|\mathcal{F}_t) \cdot c_{1,2}(u_1, u_2|\mathcal{F}_t) \cdot c_{1,3}(u_1, u_3|\mathcal{F}_t) \\
&\times c_{1,4}(u_1, u_4|\mathcal{F}_t) \cdot c_{2,3|1}(u_{2|1}, u_{3|1}|\mathcal{F}_t) \cdot c_{2,4|1}(u_{2|1}, u_{4|1}|\mathcal{F}_t) \cdot c_{3,4|1,2}(u_{3|1,2}, u_{4|1,2}|\mathcal{F}_t) \\
&= \prod_{k=1}^{4} f(r_k) \prod_{j=1}^{3} \prod_{i=1}^{3} c_{j,j+i|1,\ldots,j-1}(F(r_j|r_1, \ldots, r_{j-1}), F(r_{j+i}|r_1, \ldots, r_{j-1}))
\end{aligned}
$$

Drop the terms between brackets and a simplified function is obtained:

$$\begin{aligned} f_{1234} &= f_1 \cdot f_2 \cdot f_3 \cdot f_4 \cdot c_{1,2} \cdot c_{1,3} \cdot c_{1,4} \cdot c_{2,3|1} \cdot c_{2,4|1} \cdot c_{3,4|1,2} \\ &= \prod_{k=1}^{4} f\left(r_k\right) \prod_{j=1}^{3} \prod_{i=1}^{3} c_{j,j+i|1,\ldots,j-1} \\ &= c_{1,2,3,4}, \end{aligned}$$

matching the C-vine structure shown in Appendix C.1.

B.2 D-vine copula

$$\begin{aligned} f(r_1, r_2, r_3, r_4|\mathcal{F}_t) &= f_{1,4|2,3}(r_1, r_4|r_2, r_3, \mathcal{F}_t) \cdot f_{2,3}(r_2, r_3|\mathcal{F}_t) \\ &= c_{1,4|2,3}(u_{1|2,3}, u_{4|2,3}|\mathcal{F}_t) \cdot f_{1,|2,3}(r_1|r_2, r_3, \mathcal{F}_t) \cdot f_{4|2,3}(r_4|r_2, r_3, \mathcal{F}_t) \cdot f_{2,3}(r_2, r_3|\mathcal{F}_t) \\ &= c_{1,4|2,3}(u_{1|2,3}, u_{4|2,3}|\mathcal{F}_t) \cdot \frac{f_{1,3|2}(r_1, r_3|r_2, \mathcal{F}_t)}{f_{3|2}(r_3|r_2, \mathcal{F}_t)} \cdot \frac{f_{2,4|3}(r_2, r_4|r_3, \mathcal{F}_t)}{f_{2|3}(r_2|r_3, \mathcal{F}_t)} \cdot f_{2,3}(r_2, r_3|\mathcal{F}_t) \\ &= c_{1,4|2,3}(u_{1|2,3}, u_{4|2,3}|\mathcal{F}_t) \cdot c_{1,3|2}(u_{1|2}, u_{3|2}|\mathcal{F}_t) \cdot f_{1|2}(r_1|r_2, \mathcal{F}_t) \cdot c_{2,4|3}(u_{2|3}, u_{4|3}|\mathcal{F}_t) \\ &\times f_{4|3}(r_4|r_3, \mathcal{F}_t)\ f_{2,3}(r_2, r_3|\mathcal{F}_t) \\ &= c_{1,4|2,3}(u_{1|2,3}, u_{4|2,3}|\mathcal{F}_t) \cdot c_{1,3|2}(u_{1|2}, u_{3|2}|\mathcal{F}_t) \cdot \frac{f_{1,2}(r_1, r_2|\mathcal{F}_t)}{f_2(r_2|\mathcal{F}_t)} \cdot c_{2,4|3}(u_{2|3}, u_{4|3}|\mathcal{F}_t) \\ &\times \frac{f_{3,4}(r_3, r_4|\mathcal{F}_t)}{f_3(r_3|\mathcal{F}_t)} \cdot f_{2,3}(r_2, r_3|\mathcal{F}_t) \\ &= c_{1,4|2,3}(u_{1|2,3}, u_{4|2,3}|\mathcal{F}_t) \cdot c_{1,3|2}(u_{1|2}, u_{3|2}|\mathcal{F}_t) \cdot c_{1,2}(u_1, u_2|\mathcal{F}_t) \cdot f_1(r_1|\mathcal{F}_t) \\ &\times c_{2,4|3}(u_{2|3}, u_{4|3}|\mathcal{F}_t) \cdot c_{3,4}(u_3, u_4|\mathcal{F}_t) \cdot f_4(r_4|\mathcal{F}_t) \cdot f_{2,3}(r_2, r_3|\mathcal{F}_t) \\ &= c_{1,4|2,3}(u_{1|2,3}, u_{4|2,3}|\mathcal{F}_t) \cdot c_{1,3|2}(u_{1|2}, u_{3|2}|\mathcal{F}_t) \cdot c_{1,2}(u_1, u_2|\mathcal{F}_t) \cdot f_1(r_1|\mathcal{F}_t) \\ &\times c_{2,4|3}(u_{2|3}, u_{4|3}|\mathcal{F}_t) \cdot c_{3,4}(u_3, u_4|\mathcal{F}_t) \cdot f_4(r_4|\mathcal{F}_t) \cdot c_{2,3}(u_2, u_3|\mathcal{F}_t) \cdot f_2(r_2|\mathcal{F}_t) \cdot f_3(r_3|\mathcal{F}_t), \\ &= c_{1,2,3,4}(u_1, u_2, u_3, u_4|\mathcal{F}_t), \end{aligned}$$

where $u_i = F_i(r_i|\mathcal{F}_t)$ and $u_{i|j} = F_{i|j}(r_i|r_j, \mathcal{F}_t)$ with $i = 1, \ldots, 4; i \neq j$. Rearranging the terms such that the most basic functions are in the front, gives

$$\begin{aligned} f(r_1, r_2, r_3, r_4|\mathcal{F}_t) &= f_1(r_1|\mathcal{F}_t) \cdot f_2(r_2|\mathcal{F}_t) \cdot f_3(r_3|\mathcal{F}_t) \cdot f_4(r_4|\mathcal{F}_t) \cdot c_{1,2}(u_1, u_2|\mathcal{F}_t) \cdot c_{2,3}(u_2, u_3|\mathcal{F}_t) \\ &\times c_{3,4}(u_3, u_4|\mathcal{F}_t) \cdot c_{1,3|2}(u_{1|2}, u_{3|2}|\mathcal{F}_t) \cdot c_{2,4|3}(u_{2|3}, u_{4|3}|\mathcal{F}_t) \cdot c_{1,4|2,3}(u_{1|2,3}, u_{4|2,3}|\mathcal{F}_t) \\ &= \prod_{k=1}^{4} f\left(r_k\right) \prod_{j=1}^{3} \prod_{i=1}^{3} c_{i,i+j|i+1,\ldots,i+j-1}\big(F(r_i|r_{i+1}, \ldots, r_{i+j-1}), F(r_{i+j}|r_{i+1}, \ldots, r_{i+j-1})\big) \end{aligned}$$

Drop the terms between brackets and a simplified function is obtained, which matches the D-vine

structure given in Appendix C.2.

$$\begin{aligned} f_{1234} &= f_1 \cdot f_2 \cdot f_3 \cdot f_4 \cdot c_{1,2} \cdot c_{2,3} \cdot c_{3,4} \cdot c_{1,3|2} \cdot c_{2,4|3} \cdot c_{1,4|2,3} \\ &= \prod_{k=1}^{4} f\left(r_k\right) \prod_{j=1}^{3} \prod_{i=1}^{3} c_{i,i+j|i+1,\ldots,i+j-1} \\ &= c_{1,2,3,4}, \end{aligned}$$

Appendix C

Structures vine copulas

C.1 C-vine copula

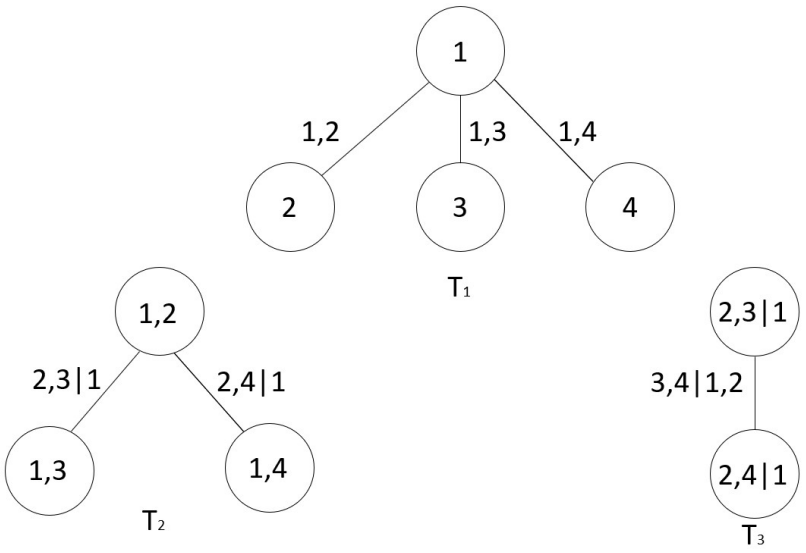

Figure C.1: Four-dimensional C-vine copula structure

C.2 D-vine copula

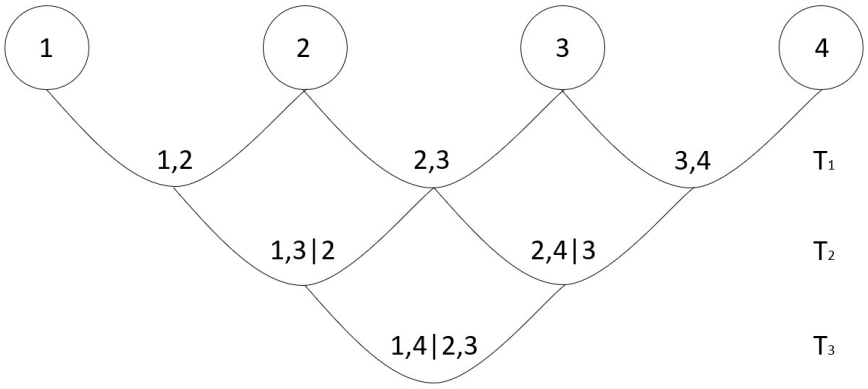

Figure C.2: Four-dimensional D-vine copula structure

Appendix D

Derivation expectation of the pseudo log-likelihood function of the energy returns and states

$$
\begin{aligned}
f(\tilde{\mathbf{r}}_T, \mathbf{S}_T|\boldsymbol{\Psi}) &= \prod_{t=1}^{T}\left[\sum_{k=1}^{2}(f(\mathbf{r}_t|S_t=k,\boldsymbol{\Psi}_{GV,k})\cdot P[S_t=k|\boldsymbol{\Psi}_{MS}])^{I_{[S_t=k]}}\right] \\
\ln\left(f(\tilde{\mathbf{r}}_T, \mathbf{S}_T|\boldsymbol{\Psi})\right) &= \sum_{t=1}^{T}\left[\sum_{k=1}^{2} I_{[S_t=k]}\Big(\ln\left(f(\mathbf{r}_t|S_t=k,\boldsymbol{\Psi}_{GV,k})\right)+\ln\left(P[S_t=k|\boldsymbol{\Psi}_{MS}]\right)\Big)\right] \\
&\mathrm{E}_{\mathbf{S}_T|\tilde{\mathbf{r}}_T,\boldsymbol{\Psi}}\Big[\ln\left(f(\tilde{\mathbf{r}}_T, \mathbf{S}_T|\boldsymbol{\Psi})\right]\Big] \\
&\qquad= \sum_{t=1}^{T}\left[\sum_{k=1}^{2}\mathrm{E}_{\mathbf{S}_T|\tilde{\mathbf{r}}_T,\boldsymbol{\Psi}}\Big[I_{[S_t=k]}\Big]\Big(\ln\left(f(\mathbf{r}_t|S_t=k,\boldsymbol{\Psi}_{GV,k})\right)+\ln\left(P[S_t=k|\boldsymbol{\Psi}_{MS}]\right)\Big)\right] \\
&\qquad= \sum_{t=1}^{T}\left[\sum_{k=1}^{2}P[S_t=k|\tilde{\mathbf{r}}_T,\boldsymbol{\Psi}]\Big(\ln\left(f(\mathbf{r}_t|S_t=k,\boldsymbol{\Psi}_{GV,k})\right)+\ln\left(P[S_t=k|\boldsymbol{\Psi}_{MS}]\right)\Big)\right] \\
&\qquad= \sum_{t=1}^{T}\left[\sum_{k=1}^{2}P[S_t=k|\tilde{\mathbf{r}}_T,\boldsymbol{\Psi}]\Big(\ln\left(f(\mathbf{r}_t|S_t=k,\boldsymbol{\Psi}_{GV,k})\right)\Big)\right] \\
&\qquad+ \sum_{t=1}^{T}\left[\sum_{k=1}^{2}P[S_t=k|\tilde{\mathbf{r}}_T,\boldsymbol{\Psi}]\Big(\ln\left(P[S_t=k|\boldsymbol{\Psi}_{MS}]\right)\Big)\right] \\
&\qquad= \sum_{t=1}^{T}\left[\sum_{k=1}^{2}\Big(\boldsymbol{\xi}_{t|T}(\boldsymbol{\Psi})\Big)_k\Big(\ln\left(f(\mathbf{r}_t|S_t=k,\boldsymbol{\Psi}_{GV,k})\right)\Big)\right] \\
&\qquad+ \sum_{t=1}^{T}\Big[P[S_t=1|\tilde{\mathbf{r}}_T,\boldsymbol{\Psi}]\ln\Big(P[S_t=1|\boldsymbol{\Psi}_{MS}]\Big)+\Big(1-P[S_t=1|\tilde{\mathbf{r}}_T,\boldsymbol{\Psi}]\Big)\ln\Big(1-P[S_t=1|\boldsymbol{\Psi}_{MS}]\Big)\Big] \\
&\mathrm{E}_{S_T|\tilde{\mathbf{r}}_T,\boldsymbol{\Psi}^c}\Big[\ln\left(f(\tilde{\mathbf{r}}_T, \tilde{\mathbf{S}}_T|\boldsymbol{\Psi}^{c+1})\right]\Big] \\
&\qquad= \sum_{t=1}^{T}\left[\sum_{k=1}^{2}P[S_t=k|\tilde{\mathbf{r}}_T,\boldsymbol{\Psi}^c]\Big(\ln\Big(f(\mathbf{r}_t|S_t=k,\boldsymbol{\Psi}^{c+1}_{GV,k})\Big)+\ln\Big(P[S_t=k|\boldsymbol{\Psi}^{c+1}_{MS}]\Big)\Big)\right] \\
&\qquad= \sum_{t=1}^{T}\left[\sum_{k=1}^{2}\Big(\boldsymbol{\xi}_{t|T}(\boldsymbol{\Psi}^c)\Big)_k\Big(\ln\Big(f(\mathbf{r}_t|S_t=k,\boldsymbol{\Psi}^{c+1}_{GV,k})\Big)\Big)\right] \\
&\qquad+ \sum_{t=1}^{T}\Big[P[S_t=1|\tilde{\mathbf{r}}_T,\boldsymbol{\Psi}^c]\ln\Big(P[S_t=1|\boldsymbol{\Psi}^{c+1}_{MS}]\Big)+\Big(1-P[S_t=1|\tilde{\mathbf{r}}_T,\boldsymbol{\Psi}^c]\Big)\ln\Big(1-P[S_t=1|\boldsymbol{\Psi}^{c+1}_{MS}]\Big)\Big] \\
&\qquad= A+B
\end{aligned}
\tag{D.1}
$$

Appendix E

Hamilton filter

I obtain the conditional probabilities of the latent states given the current parameter set $P[S_t = k|\tilde{\mathbf{r}}_T, \boldsymbol{\Psi}^c]$ by running through the three steps of the Hamilton filter shown in Table E.1. Here $\boldsymbol{\xi}_{t|t-1}$ represents the vector of conditional state probabilities at time t conditioned on the available information at time $t-1$. The first step of the Hamilton filter involves making predicitons by multiplying the state probabilities from the known previous time step $t-1$ with the transition probability matrix. Subsequently, the update step incorporates current information at time t to enhance the state probabiltites. And, lastly, the state probabilities are revised by taking all the information up until time T into consideration, resulting in smoothed state probabilities.

Table E.1: Hamilton filter procedure for a 2-state Markov switching model.

Step	**Computation**
Initialize	$\boldsymbol{\xi}_{1\|0} = \begin{pmatrix} \frac{1-p_{22}}{2-p_{11}-p_{22}} \\ \frac{1-p_{11}}{2-p_{11}-p_{22}} \end{pmatrix}$.
Prediction	While $t \leq T$, $\boldsymbol{\xi}_{t\|t-1} = \mathbf{P}'\boldsymbol{\xi}_{t-1\|t-1}$ with $\mathbf{P}$ defined as in Equation (4.4).
Update	$\boldsymbol{\xi}_{t\|t} = \begin{pmatrix} P[S_t = 1\|\tilde{\mathbf{r}}_t, \boldsymbol{\Psi}] \\ P[S_t = 2\|\tilde{\mathbf{r}}_t, \boldsymbol{\Psi}] \end{pmatrix} = \frac{\begin{pmatrix} f(\mathbf{r}_t\|S_t = 1, \tilde{\mathbf{r}}_{t-1}, \boldsymbol{\Psi}_{GV,1}) \\ f(\mathbf{r}_t\|S_t = 2, \tilde{\mathbf{r}}_{t-1}, \boldsymbol{\Psi}_{GV,2}) \end{pmatrix} \odot \boldsymbol{\xi}_{t\|t-1}}{(1 \quad 1)\left[\begin{pmatrix} f(\mathbf{r}_t\|S_t = 1, \tilde{\mathbf{r}}_{t-1}, \boldsymbol{\Psi}_{GV,1}) \\ f(\mathbf{r}_t\|S_t = 2, \tilde{\mathbf{r}}_{t-1}, \boldsymbol{\Psi}_{GV,2}) \end{pmatrix} \odot \boldsymbol{\xi}_{t\|t-1}\right]}$ with $f(\mathbf{r}_t\|S_t = k, \tilde{\mathbf{r}}_{t-1}, \boldsymbol{\Psi}_{GV,k})$ the assumed return distribution given state $k \in \{1, 2\}$ and $\odot$ the element wise multiplication of vectors.
Smooth	$\boldsymbol{\xi}_{t\|T} = \boldsymbol{\xi}_{t\|t} \oslash \mathbf{P}' \left(\boldsymbol{\xi}_{t+1\|T} \oslash \boldsymbol{\xi}_{t+1\|t}\right)$ where $\oslash$ denotes the element wise division of vectors.

Appendix F

Maximization step in the stepwise EM-algorithm

F.1 Unconditional probabilities

The unconditional probabilities in part C of Table 4.1 can be derived analytically by taking the derivative with respect to $P[S_t = 1|\mathbf{\Psi}_{MS}^{c+1}]$ and using the property that the total probability should sum up to 1, $P[S_t = 1|\mathbf{\Psi}_{MS}^{c+1}] = 1 - P[S_t = 2|\mathbf{\Psi}_{MS}^{c+1}]$,

$$\begin{aligned} P[S_t = 1|\mathbf{\Psi}_{MS}^{c+1}] &= \frac{1}{T}\sum_{t=1}^{T} P[S_t = 1|\tilde{\mathbf{r}}_T, \mathbf{\Psi}^c], \\ P[S_t = 2|\mathbf{\Psi}_{MS}^{c+1}] &= \frac{1}{T}\sum_{t=1}^{T} (1 - P[S_t = 1|\tilde{\mathbf{r}}_T, \mathbf{\Psi}^c]). \end{aligned} \tag{F.1}$$

Furthermore, the transition probabilities from Equation 4.4 can also be derived analytically. In that case the joint energy return and state function from Equation 4.9 is split in the conditional pdf of the energy returns and transition probabilities, such that $P[S_t = k|\mathbf{\Psi}_{MS}^{c+1}] = P[S_t = k|S_{t-1} = 1, \mathbf{\Psi}_{MS}^{c+1}] + P[S_t = k|S_{t-1} = 2, \mathbf{\Psi}_{MS}^{c+1}]$. For the complete derivation I refer to Stöber & Czado (2014).

$$\begin{aligned} P[S_t = 1|S_{t-1} = 1, \mathbf{\Psi}_{MS}^{c+1}] &= \frac{\sum_{t=1}^{T} P[S_t = 1, S_{t-1} = 1|\tilde{\mathbf{r}}_T, \mathbf{\Psi}^c]}{\sum_{t=1}^{T} P[S_{t-1} = 1|\tilde{\mathbf{r}}_T, \mathbf{\Psi}^c]} \\ P[S_t = 2|S_{t-1} = 2, \mathbf{\Psi}_{MS}^{c+1}] &= \frac{\sum_{t=1}^{T} P[S_t = 2, S_{t-1} = 2|\tilde{\mathbf{r}}_T, \mathbf{\Psi}^c]}{\sum_{t=1}^{T} P[S_{t-1} = 2|\tilde{\mathbf{r}}_T, \mathbf{\Psi}^c]} \end{aligned} \tag{F.2}$$

F.2 Log-likelihood functions of MS-GJR-MS-vine model for C- and D-vine copulas

The stepwise maximization presented in Algorithms 1 and 2 employ, respectively, a regime-switching GJR & C-vine with log-likelihood function

$$\begin{aligned}
&\ln\left(f(\mathbf{r}_t|\, S_t = k, \mathbf{\Psi}^{c+1}_{GV,k})\right) \\
&\quad = \sum_{i=1}^{n} \ln\Big(\phi\Big(r_{i,t}|\mu^{c+1}_{i,k}, (\sigma^{c+1}_{i,k,t})^2\Big)\Big) \\
&\quad + \sum_{j=1}^{3}\sum_{i=1}^{n-j} \ln\Big(c_{j,j+i|1,\ldots,j-1}\Big(F\left(z_{j,t}|z_{1,t},\ldots,z_{j-1,t}\right), F\left(z_{j+i,t}|z_{1,t},\ldots,z_{j-1,t}\right)|(\mathcal{V},\mathbf{C},\mathbf{\Psi}^{c+1}_{vine})_k\Big)\Big),
\end{aligned} \tag{F.3}$$

and a regime-switching GJR & D-vine with log-likelihood function

$$\begin{aligned}
&\ln\left(f(\mathbf{r}_t|\, S_t = k, \mathbf{\Psi}^{c+1}_{GV,k})\right) \\
&\quad = \sum_{i=1}^{n} \ln\Big(\phi\Big(r_{i,t}|\mu^{c+1}_{i,k}, (\sigma^{c+1}_{i,k,t})^2\Big)\Big) \\
&\quad + \sum_{j=1}^{3}\sum_{i=1}^{n-j} \ln\Big(c_{i,i+j|i+1,\ldots,i+j-1}\Big(F\left(z_{i,t}|z_{i+1,t},\ldots,z_{i+j-1,t}\right), F\left(z_{i+j,t}|z_{i+1,t},\ldots,z_{i+j-1,t}\right)|(\mathcal{V},\mathbf{C},\mathbf{\Psi}^{c+1}_{vine})_k\Big)\Big).
\end{aligned} \tag{F.4}$$

F.3 Parameters maximization step

The parameters obtained from the maximizations of the log-likelihood functions for the GJR-GARCH volatilities and the bivariate copulas collectively constitute the parameter set for the GJR-vine at iteration $c+1$: $\mathbf{\Psi}^{c+1}_{GV} = \{\mathbf{\Psi}^{c+1}_{GJR,i}, \mathbf{\Psi}^{c+1}_{vine,\{j,i\}} : \forall j, i\}$ where

$$\mathbf{\Psi}^{c+1}_{GJR,i} = \{\mu^{c+1}_{i,1}, \alpha^{c+1}_{0,i,1}, \alpha^{c+1}_{1,i,1}, \gamma^{c+1}_{i,1}, \beta^{c+1}_{i,1}, \mu^{c+1}_{i,2}, \alpha^{c+1}_{0,i,2}, \alpha^{c+1}_{1,i,2}, \gamma^{c+1}_{i,2}, \beta^{c+1}_{i,2}\} \tag{F.5}$$

and

$$\mathbf{\Psi}^{c+1}_{vine,\{j,i\}} = \{\Theta^{1,c+1}_{j,i}, \Theta^{2,c+1}_{j,i}\} \tag{F.6}$$

with $\Theta_{j,i}^{k,c+1}$ denoting the parameters of the bivariate copula i in layer j of the state k vine copula during iteration $c+1$.

Appendix G

Algorithms stepwise maximization of GJR-MS-vine model

Algorithm 3 outlines the procedure for a GJR-GARCH volatilities along with a regime-switching C-vine to connect the standardized residuals. On the other hand, Algorithm **??** shows the steps for GJR-GARCH volatilities with a regime-switching D-vine to connect the standardized residuals.

Algorithm 3 Stepwise maximization of GJR-GARCH volatilities & a regime-switching C-vine

Require: Conditional state probabilities $w_{1,t}^c = P[S_t = 1|\tilde{\mathbf{r}}_T, \mathbf{\Psi}^c]$ and $w_2^c = P[S_t = 2|\tilde{\mathbf{r}}_T, \mathbf{\Psi}^c]$

for $i \leftarrow 1, \ldots, n$ **do**

Maximize the log-likelihood of the GJR-GARCH model

$$\text{LL} = \max_{\mathbf{\Psi}_{GJR,i}^{c+1}} \left\{ \sum_{t=1}^{T} \ln \left(\phi(r_{i,t}|\mu_i^{c+1}, (\sigma_{i,t}^{c+1})^2) \right) \right\}$$

and obtain the corresponding standardized residuals: $z_{i,t} = \frac{r_{i,t}-\mu_i}{\sigma_{i,t}}$, $\forall t$.

$\mathbf{u}_{0,i}^k = F(\mathbf{z}_i)$, where $\mathbf{z}_i = (z_{i,1}, \ldots, z_{i,T})$, $\forall k$.

end for

log-likelihood = 0

for $j \leftarrow 1, \ldots, n-1$ **do**

for $i \leftarrow 1, \ldots, n-j$ **do**

$$\text{LL} = \max_{\mathbf{\Psi}_{vine,\{j,i\}}^{c+1}} \left\{ \sum_{t=1}^{T} \Big[w_{1,t}^c \ln \left(c_{j,i}^1(\mathbf{u}_{j-1,1}^1, \mathbf{u}_{j-1,i+1}^1|\Theta_{j,i}^{1,c+1}) \right) + w_{2,t}^c \ln \left(c_{j,i}^2(\mathbf{u}_{j-1,1}^2, \mathbf{u}_{j-1,i+1}^2|\Theta_{j,i}^{2,c+1}) \right) \Big] \right\}$$

log-likelihood = log-likelihood + LL

end for

if $j == n-1$ **then**

Stop

end if

for $i \leftarrow 1, \ldots, n-j$ **do**

$\mathbf{u}_{j,i}^k = h\left(\mathbf{u}_{j-1,i+1}^k, \mathbf{u}_{j-1,1}^k|\Theta_{j,i}^{k,c+1}\right)$

end for

end for

Algorithm 4 Stepwise maximization of GJR-GARCH volatilities & a regime-switching D-vine

Require: Conditional state probabilities $w_{1,t}^c = P[S_t = 1|\tilde{\mathbf{r}}_T, \mathbf{\Psi}^c]$ and $w_2^c = P[S_t = 2|\tilde{\mathbf{r}}_T, \mathbf{\Psi}^c]$

for $i \leftarrow 1, \ldots, n$ **do**

Maximize the log-likelihood of the GJR-GARCH model

$$\text{LL} = \max_{\mathbf{\Psi}_{GJR,i}^{c+1}} \left\{ \sum_{t=1}^{T} \ln\left(\phi(r_{i,t}|\mu_i^{c+1}, (\sigma_{i,t}^{c+1})^2)\right) \right\}$$

and obtain the corresponding standardized residuals per state k: $z_{i,t} = \frac{r_{i,t}-\mu_i}{\sigma_{i,t}}$, $\forall t$.

$\mathbf{u}_{0,i}^k = F(\mathbf{z}_i)$, $\forall k$, where $\mathbf{z}_i = (z_{i,1}, \ldots, z_{i,T})$.

end for

log-likelihood = 0

for $i \leftarrow 1, \ldots, n-1$ **do**

$$\text{LL} = \max_{\mathbf{\Psi}_{vine,\{1,i\}}^{c+1}} \left\{ \sum_{t=1}^{T} \Big[w_{1,t}^c \ln\left(c_{1,i}^1(\mathbf{u}_{0,i}^1, \mathbf{u}_{0,i+1}^1|\Theta_{1,i}^{1,c+1})\right) + w_{2,t}^c \ln\left(c_{1,i}^2(\mathbf{u}_{0,i}^2, \mathbf{u}_{0,i+1}^2|\Theta_{1,i}^{2,c+1})\right) \Big] \right\}$$

log-likelihood = log-likelihood + LL

end for

$\mathbf{u}_{1,1}^k = h\left(\mathbf{u}_{0,1}^k, \mathbf{u}_{0,2}^k|\Theta_{1,1}^{k,c+1}\right)$, $\forall k$

for $l \leftarrow 1, \ldots, n-3$ **do**

$\mathbf{u}_{1,2l}^k = h\left(\mathbf{u}_{0,l+2}^k, \mathbf{u}_{0,l+1}^k|\Theta_{1,l+1}^{k,c+1}\right)$, $\forall k$

$\mathbf{u}_{1,2l+1}^k = h\left(\mathbf{u}_{0,l+1}^k, \mathbf{u}_{0,l+2}^k|\Theta_{1,l+1}^{k,c+1}\right)$, $\forall k$

end for

$\mathbf{u}_{1,2n-4}^k = h\left(\mathbf{u}_{0,n}^k, \mathbf{u}_{0,n-1}^k|\Theta_{1,n-1}^{k,c+1}\right)$, $\forall k$

for $j \leftarrow 2, \ldots, n-1$ **do**

for $i \leftarrow 1, \ldots, n-j$ **do**

$$\text{LL} = \max_{\mathbf{\Psi}_{vine,\{j,i\}}^{c+1}} \left\{ \sum_{t=1}^{T} \Big[w_{1,t}^c \ln\left(c_{j,i}^1(\mathbf{u}_{j-1,2i-1}^1, \mathbf{u}_{j-1,2i}^1|\Theta_{j,i}^{1,c+1})\right) + w_{2,t}^c \ln\left(c_{j,i}^2(\mathbf{u}_{j-1,2i-1}^2, \mathbf{u}_{j-1,2i}^2|\Theta_{j,i}^{2,c+1})\right) \Big] \right\}$$

log-likelihood = log-likelihood + LL

end for

if $j == n-1$ **then**

Stop

end if

$\mathbf{u}_{j,1}^k = h\left(\mathbf{u}_{j-1,1}^k, \mathbf{u}_{j-1,2}^k|\Theta_{j,1}^{k,c+1}\right)$, $\forall k$

end for

Appendix H

Definitions Value-at-Risk and expected shortfall

The first upside risk measure is the widely used VaR. Linsmeier & Pearson (2000) provide us with a definition.

Definition H.0.1 (Value-at-Risk)**.** *With a probability of x percent and a holding period of t days, an entity's VaR is the loss that is expected to be exceeded with a probability of only x percent during the next t-day holding period. Alternatively, VaR is the loss that is expected to be exceeded during x percent of t-day holding periods.*

$$VaR_x(\pi_t) = -F_{\pi_t}^{-1}(1-x), \tag{H.1}$$

where F is the CDF corresponding to π_t*.*

Note that the CDF F in our case is a multivariate copula. However, VaR is criticized because it lacks subadditivity (Artzner et al., 1999; Tasche, 2002). Therefore, in addition to using the VaR I make use of the ES or, equivalently, the conditional VaR as an alternative risk measure.

Definition H.0.2 (Expected shortfall)**.** *The ES is the expected loss given that losses exceed the VaR. The ES at the confidence level x is given as:*

$$ES_x(\pi_t) = -E[\pi_t | \pi_t \leq -VaR_x]. \tag{H.2}$$

Appendix I

Graphs hedge effectiveness VaR and ES

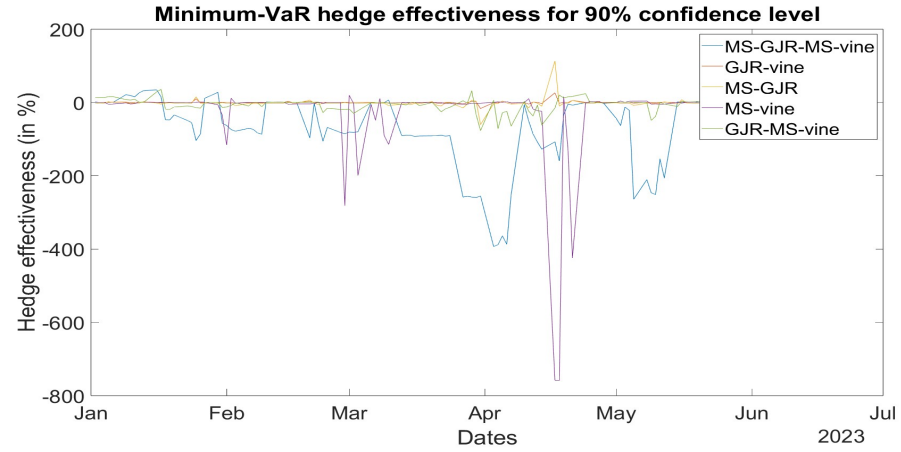

(a)

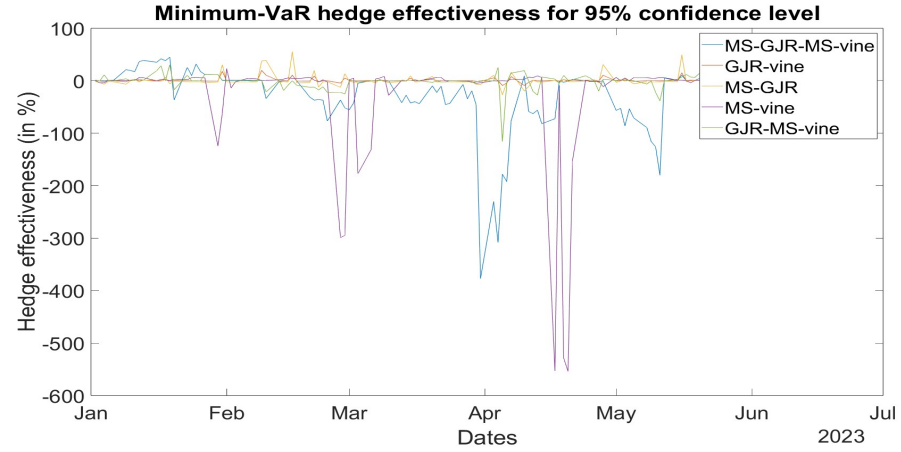

(b)

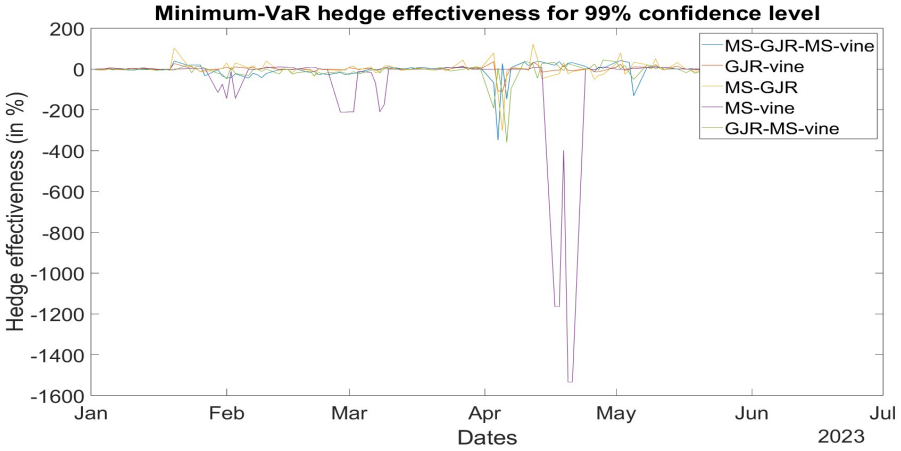

(c)

Figure I.1: Minimum-VaR hedge effectiveness (in %) for P&L-1 at confidence level 90% (I.1a), 95% (I.1b) and 99% (I.1c) over the period January 1, 2015, until June 30, 2023.

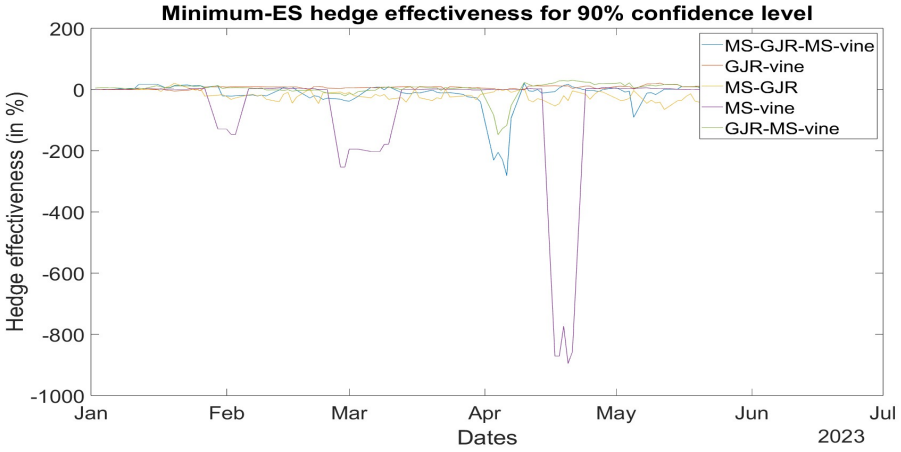

(a)

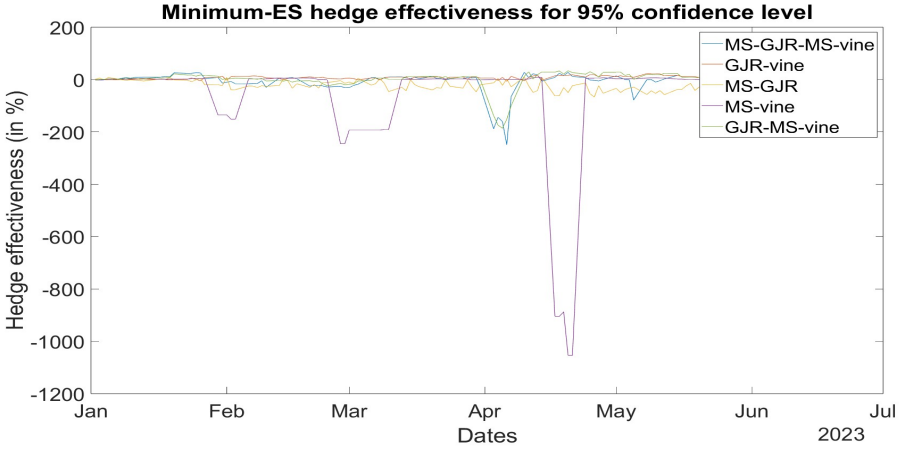

(b)

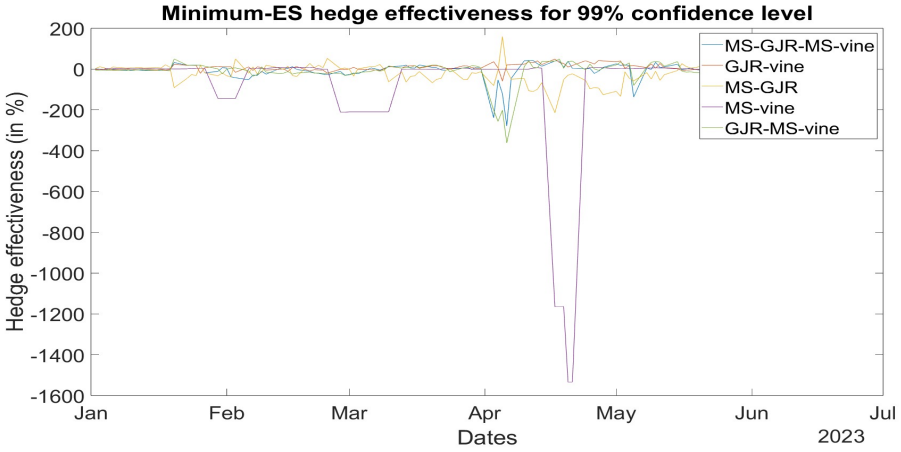

(c)

Figure I.2: Minimum-ES hedge effectiveness (in %) for P&L-1 at confidence level 90% (I.1a), 95% (I.1b) and 99% (I.1c) over the period January 1, 2015, until June 30, 2023.

Appendix J

Optimal minimum-VaR and minimum-ES hedge ratios

Table J.1: Average out-of-sample hedge ratios with the standard deviation in parentheses corresponding to minimum Value-at-Risk hedged P&L-1 to 6 for various models and confidence intervals.

	90%		95%		99%	
	$\hat{b}_1$	$\hat{b}_2$	$\hat{b}_1$	$\hat{b}_2$	$\hat{b}_1$	$\hat{b}_2$
P&L - 1						
MS-GJR-MS-vine	−0.019(0.096)**	0.071(0.039)***	−0.027(0.174)	0.053(0.030)***	−0.002(0.260)	0.038(0.026)***
GJR-vine	0.027(0.121)**	0.001(0.001)***	0.120(0.296)***	0.001(0.003)***	0.155(0.398)***	0.005(0.015)***
MS-GJR	0.148(0.109)***	−0.007(0.002)**	0.267(0.048)***	0.008(0.001)***	0.137(0.045)***	0.010(0.004)*
MS-vine	0.064(0.368)***	0.085(0.243)***	0.051(0.293)*	0.101(0.261)***	0.151(0.355)***	0.112(0.311)***
GJR-MS-vine	−0.002(0.034)	0.021(0.013)***	0.024(0.266)	0.017(0.016)***	0.035(0.269)	0.034(0.030)***
P&L - 2						
MS-GJR-MS-vine	−0.287(0.694)***	0.865(0.340)***	−0.302(0.779)***	0.857(0.358)***	−0.232(0.897)***	0.883(0.334)***
GJR-vine	0.024(0.255)	0.007(0.026)***	0.061(0.399)	−0.004(0.074)	0.115(0.670)*	0.085(0.377)**
MS-GJR	−0.301(0.190)***	0.051(0.007)***	−0.251(0.203)**	0.005(0.082)	−0.341(0.090)***	−0.001(0.001)**
MS-vine	0.005(0.060)	0.022(0.010)***	0.033(0.221)	0.020(0.014)***	0.060(0.378)	0.033(0.023)***
GJR-MS-vine	0.272(0.466)***	0.290(0.445)***	0.440(0.543)***	0.474(0.504)***	0.548(0.698)***	0.618(0.600)***
P&L - 3						
MS-GJR-MS-vine	0.634(0.211)***	0.106(0.093)**	−0.450(0.541)*	0.263(0.175)***	−0.183(0.150)*	0.491(0.302)*
GJR-vine	0.073(0.242)***	0.014(0.081)*	0.116(0.520)**	0.044(0.224)**	0.161(0.804)**	−0.115(0.698)*
MS-GJR	0.101(0.765)	0.130(0.156)**	0.703(0.286)***	0.078(0.123)**	0.459(0.039)***	0.253(0.054)***
MS-vine	−0.131(0.712)*	0.745(0.436)***	−0.287(0.791)***	0.800(0.384)***	−0.275(0.923)***	0.870(0.416)***
GJR-MS-vine	0.320(0.466)***	0.310(0.444)***	0.331(0.541)***	0.330(0.459)***	0.451(0.576)***	0.377(0.570)***
P&L - 4						
MS-GJR-MS-vine	0.821(0.350)***	0.125(0.712)*	0.085(0.032)***	0.051(0.092)*	0.350(0.132)***	0.349(0.087)***
GJR-vine	0.026(0.139)**	0.011(0.062)*	0.050(0.309)	0.026(0.130)	0.076(0.726)	0.122(0.590)**
MS-GJR	0.751(0.282)***	0.579(0.183)***	0.659(0.191)***	0.437(0.598)**	0.532(0.056)***	0.704(0.098)***
MS-vine	0.534(0.504)***	0.527(0.416)***	0.596(0.504)***	0.530(0.458)***	0.698(0.568)***	0.715(0.429)***
GJR-MS-vine	0.181(0.339)***	0.136(0.426)***	0.301(0.428)***	0.079(0.537)	0.355(0.438)***	0.456(0.580)***
P&L - 5						
MS-GJR-MS-vine	0.054(0.082)*	0.004(0.002)***	0.034(0.564)	0.039(0.012)***	0.013(0.021)**	0.059(0.019)
GJR-vine	0.001(0.000)***	0.001(0.003)**	0.001(0.001)***	0.001(0.003)***	0.001(0.002)*	0.006(0.013)***
MS-GJR	0.081(0.057)***	0.083(0.091)***	0.057(0.398)**	0.156(0.171)***	0.237(0.651)**	0.189(0.242)**
MS-vine	0.025(0.136)*	0.063(0.249)***	0.074(0.247)***	0.112(0.305)***	0.118(0.351)***	0.103(0.343)***
GJR-MS-vine	0.014(0.006)***	0.009(0.014)***	0.012(0.005)***	0.006(0.010)***	0.009(0.005)***	0.012(0.018)***
P&L - 6						
MS-GJR-MS-vine	0.062(0.035)**	0.008(0.023)*	0.179(0.275)***	0.062(0.031)***	0.258(0.148)***	0.059(0.007)***
GJR-vine	0.005(0.019)***	0.000(0.001)***	0.012(0.047)***	0.000(0.001)***	0.062(0.284)**	0.003(0.009)***
MS-GJR	0.042(0.167)*	0.495(0.157)***	0.061(0.072)***	0.183(0.475)*	0.068(0.043)***	0.062(0.036)***
MS-vine	0.004(0.009)***	0.015(0.014)***	0.006(0.012)***	0.016(0.014)***	0.014(0.020)***	0.018(0.016)***
GJR-MS-vine	0.044(0.140)***	0.009(0.007)***	0.224(0.396)***	0.012(0.012)***	0.319(0.462)***	0.035(0.026)***

Note: for every hedge ratio a t-test is performed with null hypothesis that it is equal to zero. * p < 0.10, ** p < 0.05, *** p < 0.01

Table J.2: Average out-of-sample hedge ratios with the standard deviation in parentheses corresponding to minimum Expected Shortfall hedged P&L-1 to 6 for various models and confidence intervals.

	90%		95%		99%	
	$\hat{b}_1$	$\hat{b}_2$	$\hat{b}_1$	$\hat{b}_2$	$\hat{b}_1$	$\hat{b}_2$
P&L - 1						
MS-GJR-MS-vine	0.233(0.456)	0.049(0.025)**	0.294(0.549)***	0.044(0.022)***	0.175(0.684)***	0.042(0.024)***
GJR-vine	0.543(0.321)***	0.011(0.009)**	0.827(0.267)***	0.007(0.005)***	0.611(0.485)***	0.021(0.015)***
MS-GJR	0.109(0.582)***	0.061(0.123)**	0.562(0.319)***	0.040(0.162)***	0.395(0.674)**	0.013(0.008)***
MS-vine	0.220(0.368)***	0.191(0.381)***	0.219(0.368)***	0.191(0.382)***	0.221(0.368)***	0.189(0.382)***
GJR-MS-vine	0.906(0.286)***	0.033(0.01)***	0.860(0.337)***	0.041(0.012)***	0.585(0.479)***	0.056(0.016)***
P&L - 2						
MS-GJR-MS-vine	0.967(0.212)***	0.938(0.200)***	0.827(0.541)***	0.950(0.174)***	0.405(0.903)***	0.954(0.239)***
GJR-vine	0.855(0.444)***	0.077(0.051)***	0.690(0.556)***	0.124(0.118)***	0.347(0.798)***	0.233(0.524)***
MS-GJR	0.812(0.385)***	0.071(0.298)***	0.363(0.210)***	0.895(0.637)***	0.561(0.238)***	0.157(0.129)***
MS-vine	0.890(0.309)***	0.031(0.008)***	0.899(0.298)***	0.036(0.010)***	0.629(0.481)***	0.044(0.016)***
GJR-MS-vine	0.899(0.420)***	0.048(0.015)***	0.726(0.383)***	0.060(0.019)***	0.656(0.455)***	0.079(0.022)***
P&L - 3						
MS-GJR-MS-vine	0.849(0.310)***	0.883(0.356)***	0.810(0.417)***	0.940(0.135)***	0.475(0.811)***	0.854(0.239)***
GJR-vine	0.998(0.018)***	0.615(0.458)***	0.984(0.170)***	0.523(0.733)***	0.719(0.689)***	0.168(0.949)*
MS-GJR	0.622(0.326)***	0.723(0.419)***	0.723(0.301)***	0.905(0.167)***	0.612(0.468)***	0.657(0.269)***
MS-vine	0.834(0.469)***	1.000(0.000)***	0.766(0.612)***	1.000(0.000)***	0.538(0.838)***	1.000(0.000)***
GJR-MS-vine	0.723(0.417)***	0.822(0.317)***	0.627(0.379)***	0.865(0.285)***	0.670(0.449)***	0.765(0.356)***
P&L - 4						
MS-GJR-MS-vine	0.768(0.229)***	0.848(0.280)***	0.731(0.318)***	0.823(0.321)***	0.556(0.538)***	0.623(0.434)***
GJR-vine	0.879(0.270)***	0.148(0.103)***	0.809(0.447)***	0.259(0.206)***	0.491(0.816)***	0.505(0.555)***
MS-GJR	0.549(0.412)***	0.721(0.215)***	0.410(0.347)***	0.810(0.199)***	0.425(0.671)***	0.748(0.119)***
MS-vine	1.000(0.000)***	0.969(0.137)***	1.000(0.000)***	0.981(0.087)***	0.992(0.080)***	0.999(0.016)***
GJR-MS-vine	0.824(0.302)***	0.919(0.240)***	0.712(0.347)***	0.888(0.184)***	0.622(0.508)***	0.770(0.163)***
P&L - 5						
MS-GJR-MS-vine	0.763(0.281)***	0.132(0.320)**	0.025(0.018)**	0.019(0.014)***	0.046(0.041)***	0.061(0.024)***
GJR-vine	0.001(0.001)***	0.018(0.005)***	0.001(0.001)***	0.021(0.006)***	0.001(0.003)***	0.031(0.014)***
MS-GJR	0.196(0.402)*	0.185(0.236)**	0.078(0.027)***	0.068(0.014)*	0.072(0.029)***	0.081(0.027)***
MS-vine	0.223(0.367)***	0.193(0.380)***	0.223(0.367)***	0.193(0.381)***	0.224(0.366)***	0.191(0.381)***
GJR-MS-vine	0.009(0.003)***	0.038(0.014)***	0.008(0.003)***	0.038(0.014)***	0.007(0.003)***	0.042(0.015)***
P&L - 6						
MS-GJR-MS-vine	0.756(0.271)***	0.039(0.017)***	0.717(0.315)***	0.084(0.039)***	0.537(0.548)***	0.091(0.047)***
GJR-vine	0.231(0.070)***	0.002(0.001)***	0.432(0.160)***	0.004(0.002)***	0.728(0.420)***	0.011(0.010)***
MS-GJR	0.434(0.392)***	0.048(0.025)***	0.347(0.352)***	0.024(0.019)***	0.339(0.643)***	0.079(0.017)***
MS-vine	0.037(0.021)***	0.022(0.019)***	0.037(0.021)***	0.021(0.019)***	0.037(0.024)***	0.020(0.021)***
GJR-MS-vine	0.926(0.215)***	0.015(0.005)***	0.960(0.158)***	0.028(0.008)***	0.946(0.263)***	0.051(0.016)***

Note: for every hedge ratio a t-test is performed with the null hypothesis that it is equal to zero. * $p < 0.10$, ** $p < 0.05$, *** $p < 0.01$